ResearchGate

See discussions, stats, and author profiles for this publication at: https://www.researchgate.net/publication/223026138

Experimental determination of the partitioning behavior of rare earth and high field strength elements between pargasitic amphibole and natural silicate melts

Article *in* Geochimica et Cosmochimica Acta · March 2000

DOI: 10.1016/S0016-7037(99)00379-8

CITATIONS
57

READS
194

5 authors, including:

Roger L. Nielsen
South Dakota School of Mines and Technology
124 PUBLICATIONS **3,458** CITATIONS
SEE PROFILE

James S. Beard
Virginia Museum of Natural History
83 PUBLICATIONS **4,620** CITATIONS
SEE PROFILE

Alberto E Patiño Douce
University of Georgia
55 PUBLICATIONS **6,964** CITATIONS
SEE PROFILE

Jim Blencoe
Orion Laboratories, LLC
71 PUBLICATIONS **992** CITATIONS
SEE PROFILE

Some of the authors of this publication are also working on these related projects:

I have a new interest in the origin of diamondoiferous chromitites in ophiolites. View project

Basalt petrogenesis View project

All content following this page was uploaded by Roger L. Nielsen on 10 July 2018.

The user has requested enhancement of the downloaded file.

Pergamon

Geochimica et Cosmochimica Acta, Vol. 64, No. 6, pp. 1103–1120, 2000
Copyright © 2000 Elsevier Science Ltd
Printed in the USA. All rights reserved
0016-7037/00 $20.00 + .00

PII S0016-7037(99)00379-8

Experimental determination of the partitioning behavior of rare earth and high field strength elements between pargasitic amphibole and natural silicate melts

MARK HILYARD,[1] ROGER L. NIELSEN,[1,*] JAMES S. BEARD,[2] ALBERTO PATIÑO-DOUCE,[3] and JAMES BLENCOE[4]

[1]Department of Geosciences, 104 Wilkinson Hall, Oregon State University, Corvallis, OR 97331-5506 USA
[2]Virginia Museum of Natural History, 1001 Douglas Ave., Martinsville, VA 24112 USA
[3]Department of Geology, University of Georgia, Athens, GA 30602 USA
[4]Oak Ridge National Laboratory, PO Box 2008, Building 4500-f, MS 6110, Oak Ridge, TN 37831-6110 USA

(*Received August* 12, 1997; *accepted in revised form October* 15, 1999)

Abstract—The primary goal of this investigation was to derive a set of expressions that can be used to calculate the amphibole-melt partitioning behavior of the rare earth elements (REE) and the high field strength elements (HFSE) in natural systems. To supplement the existing data set on basaltic systems, we conducted experiments on systems where amphibole was in equilibrium with dacitic, tonalitic and low Si rhyolitic melts. These experiments, doped with La, Sm, Gd, Lu, Ta, Nb, Y, Zr, and Hf, were run at pressures of 2 and 5 kbar, temperatures between 900°C and 945°C, and oxidation conditions ranging from QFM-1 to NiNiO+1.

The partitioning data obtained in this study were combined with published data to calculate two sets of expressions describing trace element partitioning. The first set models the partitioning of trace elements into amphibole using temperature, pressure and several compositional parameters, including the compositionally-compensated partition coefficients of Ti, Al, Caand SiO_2, and the exchange of Fe and Mg between the crystal and the melt (D_{Mg}/D_{Fe}). The second set of expressions are slightly less precise, but require no specific knowledge of P, T, or f_{O2} and, for application to natural systems, can be constructed solely on the basis of information available from standard electron microprobe analyses. These expressions predict amphibole-melt partition coefficients for REE and HFSE within an internal precision of 14–40% (relative) for alkali basalt to low Si rhyolite, from 850°C to 1100°C, 2–20 kbar and oxygen fugacity from QFM-1 to NiNiO+1.

Partition coefficients calculated from the expressions derived in this study were used to model the partial melting and fractional crystallization of a hypothetical amphibolite and hydrous melt, respectively. Fractionation and/or melting in amphibole-bearing systems produces a magma with a convex upward REE pattern, a characteristic common to many hornblende-bearing dacites. However, the removal or addition of an amphibole component cannot produce the strong HFSE depletion relative to the REE observed in many arc magmas. *Copyright © 2000 Elsevier Science Ltd*

1. INTRODUCTION

The group systematics of rare earth element (REE) and high field strength element (HFSE) partitioning behavior make them an important tool in petrogenetic modeling. Both groups exhibit internally coherent behavior on a gross level, with differences in partitioning behavior between individual elements within each group dominated by differences in ionic radius.

Two approaches have been adopted in the modeling of trace element partitioning. One method of determining appropriate partition coefficients is to collect them from mineral/liquid pairs in systems of specific chemical and physical conditions. This approach has the advantage that it yields relatively high levels of precision, but limits the application of the derived partition coefficients to those specific systems that have been studied in detail (see Green, 1994 review).

Another approach is to link the partitioning of trace elements with the behavior of major elements, such as Ca or Ti (Gallaghan and Nielsen, 1992; Nielsen et al., 1992; Nielsen et al., 1994; Blundy and Wood, 1994; Forsythe et al., 1994; Sisson, 1994; Klein et al., 1997; Wood and Blundy, 1997). This approach can produce models for the partitioning of trace elements that are appropriate for conditions covering a wide range of mineral/melt compositions with an equally wide range of physical parameters. However, a coherent database of partitioning data must be available for such expressions to be calculated.

To quantitatively model the differentiation of a system where the conditions are continuously changing, we must define the effects of pressure, temperature, and composition on the partitioning behavior of all elements. The partitioning of REE and HFSE into olivine, plagioclase, and pyroxene over a wide range of pressure, temperature, and compositions has been the subject of several recent investigations (McKay et al., 1986; Beattie et al., 1991; Kinzler et al., 1990; Blundy and Wood, 1991; Gallaghan and Nielsen, 1992; Forsythe et al., 1994; Hack et al., 1994; Wood and Blundy, 1997), with the result that there are now well-constrained expressions that describe the partitioning of many of the important trace elements.

The goal of this investigation was to collect a data set of experimentally-determined partition coefficients for the REE and HFSE between amphibole and andesitic to rhyolitic melts. This data set was used in conjunction with existing data on other systems (Nicholls and Harris, 1980; Green and Pearson, 1985b; Adam and Green, 1994; Sisson, 1994; Brenan et al., 1995; LaTourrette et al., 1995; Klein et al., 1997; Fujinawa and Green, 1997) to calibrate expressions describing the partitioning of these elements between amphibole and natural composition magmas ranging from alkali basalt to low-Si rhyolite.

*Author to whom correspondence should be addressed (rnielsen@oce.orst.edu).

2. THE OCCURRENCE AND STABILITY OF AMPHIBOLE

Amphibole is one of the more common phases in the crust and upper mantle. Its widespread occurrence and relatively high partition coefficients for many important trace elements makes understanding the role of amphibole critical to the development of igneous differentiation models for many systems. Amphibole occurs in ~10–40% of andesites and dacites (Ewart, 1979; Sajon et al., 1996) where in some cases, it may make up to 20 volume percent of the rock (Wones and Gilbert, 1982). Amphibole-bearing cumulate rocks have been reported as xenoliths in many arc basalts, andesites and granitoids (Cawthorn and O'Hara, 1976; Conrad and Kay, 1984; Beard, 1986; Dautria et al., 1987; Castro and Edryd, 1992; Ferreira et al., 1995; Kempton et al., 1995).

Amphibolitized peridotites and metabasites are abundant in oceanic, arc, and continental crusts, and the partial melting of these rocks can generate a wide variety of melts. Amphibole plays a critical role during melting in these systems. In fact, it is the progressive, incongruent breakdown of amphibole that typically triggers melting (Mysen and Boettcher, 1975; Spulber and Rutherford, 1983; Beard and Lofgren, 1991; Wolf and Wyllie, 1994; Patinõ-Douce and Beard, 1995; Rapp, 1995; Hartel and Pattison, 1996; Skjerlie and Johnston, 1996; Winther, 1996).

In water-saturated, andesitic to dacitic liquids, amphibole is stable to 875–975°C at P_{H2O} of 1–5 kbar (Rutherford et al., 1985; Rutherford and Devine, 1988; Beard and Lofgren, 1991). For water-saturated basaltic liquids at 2 kbar, the upper limit of amphibole stability is 985°C (Sisson and Grove, 1993), and for water-saturated basalts at pressures of 5 kbar and above, the upper stability is at least 1045°C (Helz, 1976; Allen and Boettcher, 1983; Huang and Wyllie, 1986).

During dehydration melting, the stable coexistence of amphibole and melt is a function of temperature, pressure, and bulk composition. At pressures of 2–3 kbar, amphibole plus melt may coexist from the solidus (850–900°C) to temperatures 25–50°C above the solidus. At higher pressures (>5 kbar), the amphibole plus melt field expands, and amphibole may be stable at temperatures as much as 75°C above the solidus (Rushmer, 1991; Beard and Lofgren, 1991; Patinõ-Douce and Beard, 1995; Wolf and Wyllie, 1994; Rapp and Watson, 1995). Thus, even in the absence of a vapor phase, restitic amphibole can influence melt compositions in systems that have undergone as much as 25% melting.

3. CRYSTAL CHEMISTRY

The general formula for Ca-rich amphiboles is $A_{0-1}B_2C_5T_8O_{22}(OH, F, Cl, O)_2$. In Ca-rich amphiboles, the A-site is largest (12-fold coordination) and, when occupied, is occupied by Na and K. The B-site (M4) is 8-fold coordinated and located adjacent to the A-site. In most naturally occurring amphiboles, the B-site occupied primarily by Ca and Na. The 6 fold coordinated C-sites (M1, M2, and M3) are occupied by Mg, Mn, Fe^{2+}, Fe^{3+}, Al, Cr, and Ti. The tetrahedral T-sites are occupied by Si and Al, and make up the silicate double chain framework of amphibole (Hawthorne, 1981; Leake, 1997).

The similarity of the ionic radii of the REE (0.977 Å for Lu to 1.16Å for La) and Ca (1.12Å) leads to the prediction that the REE's may substitute for Ca in the M4 site, however, the site occupancy of the HFSE is not clear. If the other HFSE behave like Ti, the M2 (C) site will be favored (Robinson et al., 1982; Leake, 1997). Recent work on the site occupancy of Ti, the REE and the HFSE (Foley et al. 1999; Oberti et al. 1999a; Oberti et al. 1999b; Tiepolo et al., 1999; Yang et al., 1999) indicates that they occupy different sites depending on the amphibole composition. For example, Foley et al. (1999) reported that Ti, Nb and Ta prefer the M1 site, and Hf and Zr occupy M2 in pargasites and M1 in richterites if dehydrogenation is present. However, expressions that describe the link between occupancy and composition have yet to be published.

4. EXISTING PARTITIONING DATA

The majority of existing partitioning data for amphibole has been the result of phenocryst/matrix determinations (e.g., Sisson, 1994), or experimental studies restricted to a narrow range of starting compositions (e.g., LaTourrette et al., 1995; Brenan et al., 1995). In an experimental investigation of the effects of pressure and temperature on partitioning for a single basanite composition, Adam and Green (1994) found that REE partitioning in amphibole was negatively correlated with pressure, and that there was less of an effect for temperature (1000°C vs. 1100°C) than pressure. In addition, Green and Pearson (1985) investigated the effect of pressure on partitioning of trace elements in an andesitic liquid at 900°C. They observed that the partitioning of REE is negatively correlated with pressure and attributed this decrease in D_{REE} to be a consequence of the flexibility of the amphibole structure, which becomes more discriminating than clinopyroxene or titanite at greater pressures. Fujinawa and Green (1997) confirmed that Zr and Hf were negatively correlated with pressure, and positively correlated with Ti in a set of follow-up experiments on andesite and basanite starting materials. They surmised that although Hf was slightly more compatible than Zr, their behavior was sufficiently similar that amphibole was not an effective mechanism for Hf/Zr fractionation.

LaTourrette et al. (1995) examined the partitioning of trace elements between amphibole and a basanite melt at 15 kbar and 1100°C, while Brenan et al. (1995) investigated trace element partitioning between amphibole and a simplified synthetic andesite melt at 15 kbar and 1000°C. In an effort to quantify the effects of pressure and temperature on partitioning, both studies modeled the partitioning into amphibole with an elastic strain model. This model was originally developed for plagioclase by Blundy and Wood (1991) and was later applied to trace element partitioning for clinopyroxene (Wood and Blundy, 1997) in anhydrous systems.

Klein et al. (1997) investigated the partitioning of REE and HFSE between amphibole and tonalitic melt at 1 GPa and low temperature (800°C, 850°C, and 900°C). Partition coefficients, when modeled in terms of both melt structure and elastic strain, fell along the predicted Onuma curves. In addition, Klein et al. (1997) found that the partitioning of the REE correlated with D_{Ti}, and was collinear with partition coefficients obtained in previous studies (Adam and Green, 1994; Brenan et al., 1995; LaTourrette et al., 1995). They also found that the slope of the DREE–D_{Ca}, correlation was different from the results of other studies.

Sisson (1994) used in situ ion-microprobe analyses of crys-

Table 1. Starting compositions used in this study

	T-85	AT4	557	478	ABA
SiO_2	45.50	48.62	57.02	52.47	49.04
TiO_2	4.11	0.91	0.60	1.74	1.27
Al_2O_3	15.04	17.38	15.39	15.29	16.37
Fe_2O_3	13.84	6.21	—	—	1.92
FeO	—	4.19	8.01	11.79	7.45
MnO	0.18	0.13	0.17	0.22	0.18
MgO	5.12	7.66	5.52	5.29	7.45
CaO	10.95	11.64	9.20	9.21	10.81
Na_2O	3.5	2.44	2.54	2.55	3.42
K_2O	1.85	0.63	0.44	0.16	0.44
P_2O_5	0.14	0.19	0.18	0.49	0.16

T85—fractionated alkaline basalt from Tahiti T85 (Duncan et al., 1994).

AT4—high-alumina basalt from the Aleutian Islands (Beard and Lofgren, 1992).

557—low-K calc-alkaline andesite (Beard and Lofgren, 1991).

478—greenstone of calc-alkaline andesite composition (Beard and Lofgren, 1991).

ABA—Alkali basaltic amphibolite (Rushmer, 1991).

tals and glass to investigate the effects of composition on the partitioning of trace elements between amphibole and melts of basaltic andesite to high-silica rhyolite composition. Partition coefficients were calculated from values obtained from phenocryst separates and remelted quench-crystallized matrix. He found that the partitioning of trace elements into hornblende was strongly correlated to D_{Ca}.

While the aforementioned studies have investigated the partitioning between amphibole and trace elements over a wide range of conditions, no single investigation has systematically examined the magnitude of each of the parameters that affect partitioning over the full range of conditions where amphibole is stable.

5. EXPERIMENTAL PROCEDURE

5.1. Starting Compositions

A set of natural starting compositions was chosen for this study to produce a wide range of melt compositions (Table 1). Each starting composition was powdered and doped with approximately 0.5 wt.% each of the dopant components (e.g., 0.5 wt% La, Lu and Hf). The doped powders were subsequently fused at 1 atm., 1200°C, quenched, ground, reheated and re-ground. Three different dopant mixtures (1) LLH–La, Lu, Hf; (2) NST–Nb, Sm, Ta; and (3) YZG–Y, Zr, Gd were used in order to avoid interferences during microprobe analysis, and to keep concentrations sufficiently low to inhibit the crystallization of REE and HFSE bearing accessory phases.

5.2. Use of Dopants

Experimental determination (versus phenocrysts/matrix) of partition coefficients offers the advantages that pressure and temperature are controlled. However, the size of crystals generated with experimental techniques was often small (~3–10 micron), making them difficult to analyze by available analytical equipment (e.g., ion probe) capable of detecting trace elements in natural abundances. The problem of small crystal size can be mitigated by doping an experiment to levels that permit the use of an electron microprobe. The benefit of in situ analysis is that inclusions of trace phases can be detected and avoided with back scatter imaging (Michael, 1988). The amount of dopant added to our charges (0.5 wt.%) is enough to be measured by the electron microprobe, yet sufficiently dilute to fall within the bounds of Henry's Law behavior (Drake and Holloway, 1981; Watson, 1985; Gallaghan and Nielsen, 1992; Beattie, 1994).

A great deal of thought and experiment has been devoted to the issue of the Henry's Law limit over the past 30 years. However, recent analytical and experimental work (Nielsen et al., 1992; Beattie, 1994; Forsythe et al., 1994) has demonstrated that Henrian behavior is the norm rather than the exception in most important natural mineral-melt systems. Therefore, the discussion below assumes that the activity coefficients exhibit behavior consistent with Henry's Law and are not a function of concentration.

5.3. Experimental Technique

The experiments were conducted at Virginia Polytechnic Institute and State University (VPI) and Oak Ridge National Laboratories in internally-heated pressure vessels (IHPV). All experiments conducted at VPI were run in 100% argon pressure medium, with pressure (± 0.1 kbar) monitored by a manganin cell and temperature (± 7°C) monitored by three chromel-alumel thermocouples. Oxygen fugacity was not buffered or monitored, but in such systems it is typically about 1 log unit above the Nickel-Nickel Oxide (NiNiO) buffer (e.g., Patinõ-Douce and Beard, 1995). The experiments conducted at Oak Ridge were run in a reducing environment of 96% argon and 4% hydrogen, equivalent to an oxygen fugacity one log unit below the quartz–fayalite–magnetite buffer (QFM-1). Pressure was monitored by calibrated Heise gauge and temperature by type-S thermocouples. Run times were 70–100 h.

For each IHPV experiment, approximately 10–30 mg of powdered starting material was loaded into gold capsules with enough water to saturate (~10 wt. H_2O). All charges were weighed before and after the experiment and all yielded fluid upon opening. Experiments were brought to run temperature with minimal overshoot, and quenched by turning the power off. Quench time was approximately 20–40 sec.

5.4. Analytical Technique

Major, minor and trace element analyses were conducted with the CAMECA SX-50 four-spectrometer electron microprobe at Oregon State University. Analysis of the amphibole crystals was performed with a 15kV accelerating voltage and a 30 nA beam current. Glass analyses were conducted with a partially defocused beam (~5–10 μ) and a 10 nA beam current during acquisition of the Na signal to mitigate Na migration during analysis. The rest of the elements in the glass were analyzed at 30 nA. Peak counting times were 10 sec. on major elements. Ti was counted for 60 sec. and 300 sec. counting times were used for the trace elements. Original Na concentration levels in the glasses were estimated by extrapolating the rate of sodium loss back to time zero as described in Nielsen and Sigurdsson (1981).

Major elements were calibrated with Smithsonian standard reference materials (Jarosewich et al., 1980). The trace elements, Y, Nb, La, Lu were calibrated on a synthetic standard (Hfrest—Patinõ-Douce et al., 1994). Hf and Zr were calibrated on the USNHM Zircon standard (117288-3), while Sm and Gd were calibrated using the REE standard of Drake and Weill (1972).

Water content of the glass in each charge was assumed to be the difference between totals obtained via the electron microprobe and 100 (Anderson, 1974; Garcia et al., 1979; Beard and Lofgren, 1991) and were calculated after the Na values were calculated. Point acquisition was documented on backscattered electron images (BSE). Glass analyses are averages of a number of point analyses in each of several glass patches in each charge (Table 2).

One of the concerns during analysis of these experiments was that the beam sampling volume might be larger than the volume of a single small amphibole crystal or glass patch. Any wandering of the beam off of the crystal during analysis results in the fluorescence of more than one phase, creating a "hybrid" analysis of glass and amphibole. To identify such erroneous results, the data were plotted against Ca, Al, and Ti. This combination of elements was found to be sufficient to discriminate between analyses of a single phase and analyses of more than one phase based on several criteria. This was effective even in the worst cases, as in the low f_{O2} experimental results, characterized by small crystal size, abundant inclusions of HFSE-rich ilmenite, and a high crystal content. Ca and Al were found to be reliable indicators for plagioclase and glass overprint on the data due to the large difference

Table 2. Electron microprobe analyses of experimentally produced amphibole and glass. LLH–La, Lu, Hf; NST–Nb, Sm, Ta; YZG–Y, Zr, Gd. n–number of analyses on which the average is based. [a] Run at QFM-1 at Oak Ridge National Laboratory. 2σ standard deviations are presented in parentheses (e.g. 40.13 (84) equals 40.13 $\pm$0.84). Error is calculated as the standard deviation of n analyses. Amphibole H_2O is calculated on the basis of stoiciometry as per Deer et al. (1992). Difference between total and 100% for glasses is assumed to be H_2O. Phase proportions are given in the order—amphibole, plagioclase, magnetite and glass unless otherwise noted.

	T85LLH	ABALLH	478LLH	AT4LLH	557LLH	T85LLH	T85LLH	ABALLH	478LLH	557LLH
P (kbar)	5	5	5	5	5	2	2	2	2	2
T(°C)	940	940	940	940	940	945[a]	940	940	940	940
amph n	15	30	11	14	5	15	14	16	11	6
SiO_2	40.13 (84)	41.99 (60)	42.77 (86)	41.89 (53)	45.32 (41)	40.17 (66)	39.25 (58)	42.92 (31)	45.27 (59)	44.25 (47)
TiO_2	3.53 (27)	2.02 (9)	2.55 (10)	1.50 (12)	1.21 (8)	4.40 (22)	3.99 (16)	2.31 (7)	2.42 (12)	1.12 (8)
Al_2O_3	14.23 (40)	14.52 (23)	13.30 (68)	14.21 (31)	12.88 (21)	13.33 (43)	12.80 (28)	12.60 (38)	10.08 (27)	11.01 (76)
FeO	11.44 (85)	10.70 (60)	11.74 (39)	12.32 (62)	12.19 (64)	12.54 (81)	10.38 (61)	9.15 (31)	10.66 (53)	11.99 (66)
MnO	0.19 (2)	0.18 (2)	0.21 (3)	0.22 (2)	0.21 (2)	0.17 (3)	0.25 (3)	0.20 (2)	0.27 (4)	0.27 (4)
MgO	12.45 (97)	13.96 (43)	13.60 (48)	12.81 (63)	13.03 (61)	11.18 (46)	13.22 (43)	15.81 (40)	15.53 (39)	15.49 (67)
CaO	11.99 (18)	11.86 (20)	10.91 (24)	11.44 (30)	11.04 (16)	11.76 (28)	12.10 (38)	11.36 (12)	10.34 (22)	9.73 (14)
K_2O	1.35 (8)	0.30 (2)	0.11 (1)	0.51 (3)	0.21 (1)	1.07 (4)	1.22 (10)	0.27 (2)	0.08 (1)	0.11 (5)
Na_2O	2.18 (12)	2.51 (7)	2.32 (7)	2.28 (6)	1.93 (3)	2.30 (7)	2.29 (8)	2.57 (6)	2.34 (87)	1.38 (9)
La_2O_3	0.12 (2)	0.11 (3)	0.09 (2)	0.06 (1)	0.06 (2)	0.19 (4)	0.13 (2)	0.21 (3)	0.09 (1)	0.25 (4)
Lu_2O_3	0.23 (3)	0.24 (2)	0.40 (4)	0.27 (3)	0.38 (3)	0.32 (4)	0.52 (10)	0.67 (4)	1.57 (8)	1.22 (8)
HfO_2	0.32 (4)	0.29 (4)	0.26 (4)	0.28 (5)	0.18 (3)	0.57 (6)	0.32 (6)	0.35 (8)	0.24 (3)	0.56 (5)
totals	99.91	100.27	99.93	99.6	99.89	99.79	98.33	99.98	100.10	99.12
H_2O	1.75	1.59	1.67	1.81	1.25	1.79	1.86	1.56	1.21	1.74
min. prop.	55 0 5 40	50 0 2 48	40 0 5 55	35 20 5 40	20 10 2 68	50 0 5 45	40 20 10 30	50 20 5 25	35 30 5 30	30 10 5 65
glass n	27	29	8	12	15	12	19	21	13	30
SiO_2	60.23 (96)	59.32 (65)	60.03 (84)	61.17 (94)	63.71 (86)	61.18 (56)	56.00 (55)	59.12 (71)	61.14 (94)	59.88 (90)
TiO_2	0.34 (5)	0.33 (6)	0.58 (4)	0.23 (4)	0.27 (7)	0.61 (9)	1.01 (21)	0.58 (8)	0.87 (5)	0.41 (7)
Al_2O_3	18.56 (27)	19.53 (32)	18.22 30)	18.18 (28)	17.15 (18)	19.55 (22)	19.01 (11)	17.57 (37)	17.87 (31)	18.35 (24)
FeO	1.17 (30)	1.44 (32)	2.06 (17)	1.14 (20)	1.73 (19)	1.56 (19)	1.83 (21)	2.19 (24)	2.09 (11)	2.55 (16)
MnO	0.11 (2)	0.11 (3)	0.13 (3)	0.12 (3)	0.08 (3)	0.10 (2)	0.13 (2)	0.12 (3)	0.11 (4)	0.08 (3)
MgO	0.03 (2)	0.15 (13)	0.23 (11)	0.07 (11)	0.29 (25)	0.05 (3)	0.15 (1)	0.45 (18)	0.58 (26)	0.49 (16)
CaO	5.51 (20)	6.48 (16)	6.15 (16)	5.42 (16)	5.19 (14)	3.50 (23)	4.43 (17)	4.34 (40)	5.44 (30)	5.44 (15)
K_2O	0.83 (12)	0.22 (4)	0.20 (6)	0.55 (5)	0.27 (9)	1.42 (36)	2.78 (28)	0.83 (20)	0.29 (3)	0.52 (6)
Na_2O	5.02 (50)	4.44 (67)	4.10 (46)	3.77 (37)	3.41 (21)	4.73 (61)	3.57 (33)	5.14 (38)	4.12 (28)	3.51 (23)
P_2O_5	0.33 (7)	0.31 (5)	0.33 (7)	0.33 (5)	0.13 (3)	0.23 (7)	0.44 (7)	0.32 (4)	0.29 (5)	0.10 (3)
La_2O_3	0.46 (5)	0.73 (8)	0.61 (9)	0.24 (8)	0.18 (2)	0.32 (6)	0.72 (6)	1.26 (11)	0.93 (4)	0.77 (4)
Lu_2O_3	0.15 (3)	0.21 (2)	0.34 (3)	0.18 (3)	0.21 (5)	0.16 (4)	0.59 (4)	0.50 (7)	0.88 (13)	0.51 (11)
HfO_2	0.28 (4)	0.35 (5)	0.37 (4)	0.29 (4)	0.19 (3)	0.33 (6)	0.35 (2)	0.49 (4)	0.54 (4)	0.41 (4)
totals	93.02	93.62	93.35	91.69	92.81	93.74	91.01	92.91	95.15	93.02

in the Ca contents of amphibole and glass (12 oxide wt.% and 4 oxide wt.% respectively), and the difference in the Al content between amphibole and plagioclase (~13% oxide and ~22% oxide respectively). Ti was used as an indicator of overprint from oxide inclusions. Note that although the full range of values for a specific experiment may vary by as much as 30%, the standard deviation of multiple determinations is significantly less.

6. THEORY

6.1. General Constraints

The partitioning of an element between silicate melt and crystal is a function of both the major element composition of the phases and the activity of the trace element components. Under normal circumstances, where the activities of the components and the substitution mechanisms are not well known, distribution coefficients ($^{xl/melt}D_{M^*} = {}^{xl}X_{M^*}/{}^{melt}X_{M^*}$), are used as measures of the trace element partitioning between phases, where $^{xl}X_{M^*}$ is the mole fraction of element M in the crystal (xl) or the melt phase (note: this designation is as opposed to $^{xl/melt}D_M$, the ratio of weight %, Beattie et al, 1993). However, partitioning is known to be dependent on composition as well as pressure and temperature. It has long been shown that components do not behave ideally in natural systems, as demonstrated by the wide range of D exhibited at a given temperature for compositionally diverse systems (see review by Green, 1994).

Ideally, the partitioning of an element between phases is best described by the equilibrium constant for the reaction by which the mineral component is formed. For example the formation of a Zr-bearing amphibole from a silicate melt could be described by the following reaction:

$$[NaO_{0.5} + 2\,CaO + 4\,MgO + ZrO_2 + 5\,SiO_2 + 3\,AlO_{1.5} + H_2O]^{melt} = [(NaCa_2)(Mg_4Zr)(Si_5Al_3)O_{22}(OH)_2]^{xtl} \quad (1)$$

The equilibrium constant for this reaction can be written as:

$$K_{eq} = \frac{a_{Amp(NaCa_2)(Mg_4Zr)(Si_5Al_3)}}{(a^{melt}_{Na_{0.5}})(a^{melt}_{CaO})^2(a^{melt}_{MgO})^4(a^{melt}_{ZrO_2})(a^{melt}_{SiO_2})^5(a^{melt}_{AlO_{1.5}})^3(a^{melt}_{H_2O})} \quad (2)$$

Under conditions of constant pressure and temperature, the activity (a) of each element in each phase is related to concentration (X) by an activity coefficient (γ), where ($a = X\gamma$). The activity of water in this case is assumed to be one. However, as noted above, the activity coefficients for trace elements in amphibole are not known. In addition, the stoichiometry of the formation of Zr amphibole (# of Al, Si, Ca atoms atoms/cell) is unknown.

While the compositional dependency of activity coefficients for some elements in a silicate melt can be reduced (Nielsen and Dungan, 1983; Ghiorso and Sack, 1995), the behavior of Al, Ti, and most trace elements in amphibole is poorly understood, both in terms of their component activities, and in terms of how they interact (e.g., nature of paired substitutions). In spite of the complexity exhibited by trace

Table 2. (Continued)

	478LLH	557LLH		T85NST	ABANST	478NST	AT4NST	557NST	T85NST	T85NST
P (kbar)	2	2		5	5	5	5	5	2	2
T(°C)	900	900		940	940	940	940	940	945[a]	940
amph n	22	22		8	26	18	26	29	12	12
SiO_2	44.47 (91)	45.56 (73)	SiO_2	40.73 (59)	41.13 (96)	43.89 (91)	42.13 (66)	42.68 (60)	40.10 (58)	41.48 (51)
TiO_2	2.70 (19)	1.57 (10)	TiO_2	2.77 (11)	1.95 (7)	2.02 (26)	1.36 (10)	1.10 (7)	4.23 (18)	3.59 (12)
Al_2O_3	11.48 (48)	10.72 (31)	Al_2O_3	14.25 (23)	14.15 (25)	13.20 (37)	14.31 (24)	12.21 (40)	13.52 (45)	12.45 (38)
FeO	11.39 (88)	10.47 (57)	FeO	11.38 (49)	10.15 (57)	13.47 (42)	10.76 (21)	10.79 (36)	12.96 (74)	10.49 (45)
MnO	0.27 (3)	0.22 (3)	MnO	0.24 (4)	0.15 (2)	0.27 (2)	0.19 (3)	0.17 (2)	0.19 (3)	0.29 (3)
MgO	14.29 (64)	16.15 (46)	MgO	12.03 (43)	14.58 (44)	11.84 (81)	13.62 (26)	15.16 (37)	11.30 (44)	13.66 (53)
CaO	10.64 (27)	10.74 (30)	CaO	11.96 (16)	11.93 (14)	11.15 (34)	11.62 (22)	11.61 (17)	11.42 (24)	11.32 (13)
K_2O	0.08 (1)	0.15 (2)	K_2O	1.29 (2)	0.29 (2)	0.09 (1)	0.49 (2)	0.23 (1)	1.04 (9)	1.11 (13)
Na_2O	2.23 (10)	1.92 (24)	Na_2O	2.16 (3)	2.45 (4)	2.23 (9)	2.23 (6)	2.01 (6)	2.33 (5)	2.34 (7)
La_2O_3	0.16 (3)	0.17 (3)	Nb_2O_5	0.09 (1)	0.20 (2)	0.22 (5)	0.22 (2)	0.19 (4)	0.31 (3)	0.22 (3)
Lu_2O_3	0.73 (4)	0.62 (3)	Sm_2O_3	0.16 (2)	0.34 (2)	0.34 (4)	0.33 (4)	0.44 (2)	0.43 (6)	0.18 (1)
HfO_2	0.43 (6)	0.28 (3)	Ta_2O_5	0.07 (1)	0.16 (3)	0.16 (5)	0.16 (4)	0.16 (4)	0.32 (4)	0.21 (4)
Total	100.58	100.29	Total	98.86	99.08	100.58	99.07	98.58	99.95	99.20
H_2O	1.71	1.72	H_2O	1.73	1.60	1.70	1.65	1.83	1.80	1.86
min prop	35 40 5 20	35 35 5 25		50 0 5 45	50 0 2 48	40 0 5 55	30 30 5 35	25 10 3 62	50 0 5 45	40 20 10 30
glass n	18	25	n	18	19	21	21	29	15	6
SiO_2	65.39 (75)	65.44 (86)	SiO_2	58.62 (91)	57.68 (81)	62.55 (90)	55.76 (86)	61.46 (89)	61.26 (70)	59.96 (31)
TiO_2	0.61 (6)	0.35 (4)	TiO_2	0.21 (6)	0.36 (5)	0.36 (10)	0.26 (6)	0.25 (5)	0.70 (13)	0.87 (28)
Al_2O_3	16.00 (32)	15.15 (23)	Al_2O_3	19.34 (27)	19.21 (42)	17.78 (28)	19.14 (33)	17.87 (20)	19.45 (16)	18.23 (24)
FeO	1.73 (36)	1.98 (44)	FeO	0.92 (13)	1.49 (22)	1.80 (63)	1.56 (35)	1.61 (39)	1.58 (24)	1.78 (51)
MnO	0.12 (3)	0.09 (2)	MnO	0.10 (3)	0.13 (3)	0.11 (3)	0.15 (3)	0.09 (3)	0.13 (4)	0.14 (3)
MgO	0.52 (40)	0.37 (14)	MgO	0.01 (1)	0.06 (4)	0.19 (21)	0.07 (3)	0.15 (8)	0.06 (5)	0.22 (23)
CaO	3.87 (25)	3.24 (16)	CaO	4.93 (13)	6.96 (20)	5.86 (16)	7.09 (23)	5.62 (15)	3.73 (23)	2.79 (30)
K_2O	0.19 (2)	0.28 (6)	K_2O	0.73 (10)	0.20 (2)	0.11 (2)	0.33 (6)	0.20 (4)	1.42 (13)	3.54 (12)
Na_2O	3.84 (21)	5.04 (18)	Na_2O	5.09 (26)	5.43 (49)	3.85 (36)	3.89 (24)	3.55 (28)	4.60 (56)	1.95 (4)
P_2O_5	0.37 (5)	0.14 (3)	P_2O_5	0.23 (5)	0.33 (5)	0.23 (5)	0.40 (7)	0.12 (3)	0.26 (5)	0.25 (51)
La_2O_3	0.48 (3)	0.74 (6)	Nb_2O_5	0.13 (2)	0.98 (4)	0.42 (3)	0.90 (7)	0.67 (7)	0.31 (3)	0.30 (3)
Lu_2O_3	0.39 (5)	0.30 (5)	Sm_2O_3	0.05 (1)	0.28 (4)	0.15 (2)	0.25 (4)	0.27 (3)	0.12 (2)	0.09 (1)
HfO_2	0.35 (3)	0.39 (4)	Ta_2O_5	0.07 (3)	0.69 (5)	0.28 (3)	0.59 (5)	0.53 (7)	0.20 (3)	0.39 (8)
Total	93.86	93.42	Total	90.43	93.8	93.69	90.39	92.39	93.82	90.51

element partitioning in amphibole noted by previous studies, the evidence that such complexity is systematic suggests that the partitioning of trace elements into amphibole can be quantitatively modeled (e.g., Nicholls and Harris, 1980; Green and Pearson, 1985; McKay et al., 1986; Blundy and Wood, 1991; Gallaghan and Nielsen, 1992; Adam and Green, 1994; Forsythe et al., 1994; Hack et al., 1994, Brenan et al., 1995; LaTourrette et al., 1995; Wood and Blundy, 1997; Foley et al., 1999; Oberti et al., 1999a; Oberti et al., 1999b).

6.2. Crystal–Chemical Effects

Partitioning of an element into a specific crystallographic site is dependent on both the ionic radius and charge (Goldschmidt, 1937; Onuma et al., 1968; Brice, 1975; Blundy and Wood, 1994; Wood and Blundy, 1997) and is reflective of the amount of strain induced upon substitution of that ion. Stated simply, those cations that are closest to the optimal radius for the site will produce the least amount of strain in the crystal lattice, resulting in a high partition coefficient for that element. As the difference in radius between substituting cations and crystallographic sites increases, so does the crystal strain, resulting in low partition coefficients for that element.

Assuming that the activity-composition relationships are the same for both major and trace-elements, a crystal-melt partition coefficient can be expressed as:

$$D = D_o \exp(-\Delta G_{rxn}/RT) \quad (3)$$

where D_o is a constant that represents the optimum partition coefficient for an unstrained site at a given pressure, temperature and composition, R is the gas constant and T is absolute temperature. Assuming that the predominant contribution to the free energy of this reaction is ΔG_{strain}, then from Brice (1975) and Eqn. (3):

$$\log D = \log D_o - 4\pi N_A E/2.303RT[r_o/2(r_i - r_o)^2 + 1/3(r_i - r_0)^3] \quad (4)$$

where N_A is Avogadro's number, E is Young's Modulus, r_i is the ionic radius of a trace element in a given site, and r_o is the optimum ionic radius for the site. This expression provides a physical basis for the correlation between the partition coefficient and ionic radii and can be used to calculate the partition coefficient as a function of r and E. Partition coefficients plotted versus radius define a parabola with a maximum describing the optimal partition coefficient and optimal site radius. E is a function of the half-width of the parabola. The wider the parabola, the more flexible the site. A rigid site is defined by a parabola with steep limbs, indicating that small changes in radius will result in greater variations of D. This relationship is illustrated in a comparison of the relatively flexible M4 site to the more rigid M1–3 sites (Comodi et al., 1991).

Partition coefficients can be predicted with this model, assuming that information about the partitioning behavior of major elements is known. For example the partitioning of other divalent cations (Sr, Ba) into the M4 site can be predicted with knowledge of D_{Ca} as in the following expression (Brenan et al., 1995):

$$\log D_i = \log D_{Ca} - 4\pi N_A E/2.303\,RT\,[r_{Ca}/2(r_{Ca} - r_i)^2 + 1/3(r_{Ca} - r_i)^3] \quad (5)$$

where r_i is the radius of the ion of interest. In addition, the partitioning of the trivalent REE cations into any appropriate site may be modeled with the knowledge of D_{Ca} and the ratio of optimal partition coeffi-

Table 2. (Continued)

	478NST	AT4NST	557NST	478NST	557NST		ABAYZG	478YZG	AT4YZG	557YZG
P (kbar)	2	2	2	2	2		5	5	5	5
T(°C)	940	940	940	900	900		940	940	940	940
amph n	9	14	21	15	15		21	23	24	15
SiO_2	45.05 (32)	43.52 (41)	46.95 (92)	44.19 (77)	46.71 (83)	SiO_2	40.68 (61)	42.25 (79)	41.54 (56)	43.92 (68)
TiO_2	2.36 (18)	1.53 (13)	1.33 (11)	2.39 (15)	1.37 (12)	TiO_2	1.92 (12)	2.28 (10)	1.52 (9)	1.29 (10)
Al_2O_3	10.43 (42)	11.65 (36)	9.96 (22)	10.99 (29)	10.05 (18)	Al_2O_3	14.09 (37)	13.24 (36)	14.54 (35)	13.16 (97)
FeO	10.64 (40)	10.11 (52)	10.75 (73)	10.36 (63)	10.89 (82)	FeO	10.88 (86)	12.39 (43)	11.9 (53)	11.37 (86)
MnO	0.28 (3)	0.23 (3)	0.24 (3)	0.29 (3)	0.24 (3)	MnO	0.18 (3)	0.23 (3)	0.21 (3)	0.19 (3)
MgO	15.52 (40)	15.07 (40)	15.93 (76)	15.46 (57)	15.79 (58)	MgO	13.29 (56)	12.76 (44)	13.35 (28)	14.29 (28)
CaO	10.48 (32)	11.16 (16)	10.93 (29)	10.93 (25)	10.88 (33)	CaO	11.74 (18)	11.51 (14)	11.58 (18)	10.85 (54)
K_2O	0.07 (1)	0.49 (5)	0.14 (1)	0.08 (1)	0.14 (1)	K_2O	0.29 (2)	0.1 (1)	0.47 (2)	0.20 (2)
Na_2O	2.12 (10)	2.21 (5)	1.73 (7)	2.24 (8)	1.76 (5)	Na_2O	2.59 (32)	2.31 (7)	2.31 (4)	1.99 (11)
Nb_2O_5	0.22 (2)	0.47 (3)	0.27 (5)	0.26 (4)	0.25 (3)	Y_2O_3	0.28 (2)	0.38 (2)	0.21 (1)	0.43 (4)
Sm_2O_3	0.45 (5)	0.37 (2)	0.44 (3)	0.53 (3)	0.46 (5)	ZrO_2	0.13 (3)	0.08 (1)	0.13 (4)	0.12 (3)
Ta_2O_5	0.19 (6)	0.39 (6)	0.20 (2)	0.18 (5)	0.19 (2)	Gd_2O_3	0.29 (2)	0.41 (2)	0.21 (2)	0.46 (4)
Total	99.89	99.03	100.72	99.75	100.43	Total	98.22	99.81	99.87	100.01
H_2O	2.08	1.83	1.85	1.85	1.70	H_2O	1.86	1.87	1.90	1.74
min prop	35 30 5 30	35 30 5 30	30 10 5 65	35 40 5 20	35 35 5 25		50 0 2 48	40 0 5 55	35 25 5 35	22 15 3 60
glass n	13	6	21	11	15	n	14	19	30	11
SiO_2	59.6 (93)	59.82 (188)	66.74 (86)	65.6 (87)	67.01 (86)	SiO_2	60.49 (85)	62.31 (105)	60.19 (170)	62.37 (65)
TiO_2	0.84 (13)	0.27 (5)	0.26 (2)	0.61 (8)	0.26 (2)	TiO_2	0.29 (10)	0.38 (15)	0.24 (6)	0.25 (4)
Al_2O_3	17.74 (28)	17.71 (28)	14.84 (30)	15.87 (29)	14.96 (30)	Al_2O_3	19.68 (21)	18.04 (22)	18.81 (54)	18.29 (18)
FeO	2.27 (39)	1.51 (17)	1.82 (25)	2.37 (67)	1.79 (25)	FeO	1.16 (28)	1.30 (22)	1.32 (23)	1.38 (12)
MnO	0.12 (3)	0.17 (5)	0.09 (2)	0.14 (3)	0.09 (2)	MnO	0.10 (3)	0.12 (2)	0.14 (4)	0.08 (3)
MgO	0.59 (23)	0.20 (7)	0.39 (6)	0.58 (32)	0.36 (6)	MgO	0.03 (2)	0.12 (9)	0.08 (9)	0.08 (2)
CaO	5.46 (29)	4.74 (39)	3.26 (4)	4.01 (18)	3.23 (4)	CaO	6.82 (23)	6.11 (21)	6.29 (25)	5.77 (19)
K_2O	0.37 (3)	0.52 (6)	0.38 (3)	0.16 (5)	0.37 (3)	K_2O	0.19 (11)	0.08 (4)	0.38 (27)	0.13 (8)
Na_2O	3.52 (18)	3.34 (29)	3.28 (22)	4.16 (22)	4.20 (22)	Na_2O	4.18 (54)	3.78 (34)	3.65 (46)	3.72 (24)
P_2O_5	0.27 (4)	0.51 (3)	0.18 (4)	0.32 (5)	0.18 (4)	P_2O_5	0.36 (4)	0.28 (5)	0.38 (8)	0.13 (3)
Nb_2O_5	0.80 (9)	0.96 (18)	0.39 (3)	0.40 (3)	0.40 (3)	Y_2O_3	0.17 (2)	0.21 (4)	0.13 (3)	0.17 (2)
Sm_2O_3	0.36 (4)	0.28 (5)	0.15 (1)	0.30 (3)	0.15 (1)	ZrO_2	0.19 (3)	0.12 (2)	0.16 (2)	0.16 (3)
Ta_2O_5	1.13 (8)	0.80 (6)	0.25 (3)	0.25 (3)	0.25 (3)	Gd_2O_3	0.14 (2)	0.17 (3)	0.10 (2)	0.14 (2)
Total	93.07	90.83	92.03	94.77	93.25	Total	93.8	93.02	91.87	92.67

cients for the 2+ and 3+ cations (D_o^{2+}/ D_o^{3+}). However, D_o, r_o and E are functions of pressure, temperature and composition of the crystal. Therefore, knowledge of all must be available to successfully model partitioning. Brenan et al. (1995) used this method to predict trace element partitioning into amphiboles (Nicholls and Harris, 1980; Green and Pearson, 1985; Dalpe et al., 1992; Dalpe et al., 1995; Adam et al., 1993; Adam and Green, 1994; Dalpe and Baker, 1994) and found that it can predict D within 40–45%.

Error is easily introduced into this model by miscalculation of appropriate pressure and temperature constants. For example, the flexibility (E) of a site is partially dependent on physical parameters of the system, as well as chemical variations (Wood and Blundy, 1997). Changes in the flexibility of the site may result in changes in the optimal radius (r_o) and partition coefficients (D_o). Perhaps more significant, expression (5) requires that the partitioning of the trace elements are correlated to Ca partitioning alone. Therefore, in application to amphibole, this approach has the weakness that it does not readily deal with variations in partitioning behavior caused by multiple substitution mechanisms possible in complex amphibole solid solutions characteristic of natural systems.

The problem of multiple substitution mechanisms and multiple site occupancy has recently been detailed by Foley et al. (1999); Tiepolo et al. (1999); Oberti et al. (1999a) and Oberti et al. (1999b). Optimally, we would require that partitioning behavior be described as a composite expression incorporating all the possible conditions. However, at present there is insufficient information on the relationships between composition, temperature, pressure, substitution mechanisms and site occupancies to treat this problem within a strictly thermodynamic framework.

6.3. Melt Component Activities

Modeling the partitioning of trace elements as a function of melt structure may approximate the melt compositional effect on REE and HFSE partitioning within amphibole (Drake and Weill, 1975; Nielsen, 1988; Nielsen, 1990). As the structure (polymerization) of a melt increases, the solubility of many trace elements decreases. Regular solution models such as those applied to major element phase equilibria (Ghiorso and Sack, 1995) can accurately model the effects of more complex component interactions. However, they are difficult to apply to trace elements due to the absence of information on the mixing properties of most trace element components.

Two commonly applied empirical methods for calculation of the effect of melt component activity on trace element partitioning are:

1. To correlate partitioning to the ratio of non-bridging oxygens to tetrahedrally coordinated cations (NBO/T) (Mysen, 1983);
2. To distribute the behavior of cations using a two-lattice melt model (Drake and Weill, 1975; Nielsen, 1985; Nielsen, 1990).

Both models assume that those cations which tend to be tetrahedrally coordinated in a melt (Si, Al) are considered to be network formers (T), while those cations which disrupt the network of a melt (Ca, Mg, Fe, Na, K), producing non-bridging oxygens (NBO) are network modifiers. In the Nielsen (1985); Nielsen, (1990) version of the two-lattice model, for peraluminous and metaluminous melts, the amount of Al which acts as a network former (tetrahedral coordination) is that which can be charge balanced by Na and K. Any excess Al is then assigned as a network modifier. In addition, it is assumed that melt components mix ideally, but only with those other melt components that have generally similar mixing properties. Specifically, the activity of network forming

Table 2. (Continued)

	T85YZG	T85YZG	T85YZG	478YZG	AT4YZG	478YZG	557YZG
P (kbar)	5	2	2	2	2	2	2
T(°C)	940	945[a]	940	940	940	900	900
amph n	12	20	5	16	15	39	6
SiO_2	40.18 (79)	40.13 (3)	40.24 (54)	44.02 (33)	45.18 (59)	44.49 (65)	44.58 (62)
TiO_2	3.66 (10)	4.76 (7)	4.07 15)	2.49 (10)	1.55 (11)	2.48 (14)	1.57 (18)
Al_2O_3	15.07 (36)	14.05 (98)	13.23 (39)	10.37 (22)	11.09 (69)	10.81 (53)	10.95 (90)
FeO	13.19 (43)	11.97 (2)	10.37 (52)	10.17 (50)	10.80 (74)	10.32 (70)	11.09 (91)
MnO	0.22 (3)	0.15 (0)	0.19 (3)	0.26 (3)	0.26 (5)	0.27 (4)	0.18 (3)
MgO	10.77 (44)	11.48 (28)	13.15 (56)	15.50 (36)	14.90 (74)	15.47 (51)	15.57 (80)
CaO	11.89 (14)	11.53 (8)	11.43 (27)	10.32 (18)	10.98 (23)	10.54 (26)	10.55 (18)
K_2O	1.28 (1)	1.20 (8)	1.21 (4)	0.08 (1)	0.59 (5)	0.08 (1)	0.14 (1)
Na_2O	2.20 (7)	2.24 (22)	2.25 (5)	2.10 (5)	2.00 (12)	2.12 (11)	1.94 (13)
Y_2O_3	0.17 (2)	0.30 (0)	0.30 (3)	0.62 (3)	0.39 (3)	0.62 (3)	0.63 (4)
ZrO_2	0.17 (1)	0.30 (3)	0.13 (3)	0.09 (2)	0.09 (1)	0.10 (2)	0.10 (3)
Gd_2O_3	0.16 (2)	0.33 (5)	0.18 (3)	0.45 (3)	0.27 (2)	0.53 (3)	0.60 (3)
Total	100.79	99.74	98.72	98.60	99.87	99.72	99.65
H_2O	1.84	1.30	1.97	2.13	1.77	1.89	1.75
min prop.	50 0 5 45	50 0 5 45	40 20 10 30	35 30 5 30	35 30 5 30	35 40 5 20	35 35 5 25
glass n	12	27	5	6	6	12	18
SiO_2	61.02 (77)	60.81 (65)	56.91 (40)	60.51 (74)	60.52 (88)	65.83 (64)	59.25 (31)
TiO_2	0.32 (13)	0.84 (31)	0.86 (3)	0.74 (12)	0.44 (8)	0.63 (9)	0.57 (2)
Al_2O_3	19.75 (39)	19.29 (40)	19.31 (35)	17.64 (34)	17.63 (44)	15.43 (42)	17.03 (2)
FeO	1.03 (26)	2.28 (75)	1.45 (40)	1.78 (29)	3.22 (84)	2.02 (20)	4.51 (38)
MnO	0.07 (2)	0.11 (3)	0.12 (12)	0.11 (2)	0.17 (4)	0.13 (3)	0.11 (3)
MgO	0.11 (20)	0.07 (4)	0.07 (24)	0.43 (23)	0.97 (67)	0.66 (24)	1.70 (2)
CaO	5.14 (35)	4.84 (37)	3.75 (23)	5.25 (27)	4.79 (42)	3.91 (43)	5.88 (2)
K_2O	0.66 (54)	0.79 (41)	3.32 (27)	0.32 (3)	1.52 (25)	0.12 (5)	0.63 (2)
Na_2O	3.88 (43)	4.50 (46)	3.67 (3)	3.17 (14)	3.45 (59)	3.78 (31)	4.10 (5)
P_2O_5	0.18 (5)	0.37 (7)	0.46 (17)	0.31 (4)	0.46 (3)	0.22 (5)	0.11 (12)
Y_2O_3	0.06 (3)	0.23 (6)	0.19 (3)	0.30 (3)	0.20 (3)	0.20 (3)	0.39 (3)
ZrO_2	0.16 (3)	0.32 (7)	0.22 (5)	0.36 (0)	0.33 (4)	0.13 (2)	0.34 (7)
Gd_2O_3	0.04 (1)	0.15 (4)	0.09 (2)	0.22 (3)	0.13 (2)	0.19 (4)	0.30 (1)
Total	92.41	94.60	90.42	91.14	93.83	93.25	94.92

components NaAl, KAl and Si and network modifying components Ca, Mg, Fe, Ti, and excess Al are equal to their mole fraction in either the network forming or modifying quasilattice.

These activities can then be applied either to the calculation of an approximate equilibrium constant (Hack et al., 1994) or to a compositionally-compensated partition coefficient where:

$$d^* = {}^{xl}X_i/({}^{melt}X_i/\Sigma NM) \quad (6)$$

where d* is the compositionally-compensated partition coefficient, ${}^{xl}X_i$ is the mole fraction of component i in the mineral, and ${}^{melt}X_i$ is the mole fraction of the component in the melt and ΣNM is the sum of the mole fractions of the network modifying components (Nielsen, 1985; Nielsen, 1990).

7. RESULTS

All runs yielded abundant (20–55% modal), small (<5–25 microns) crystals of amphibole. Crystals were generally inclusion free, with the exception of Fe–Ti oxide inclusions in amphibole in the low f_{O2} experiments, and REE oxide inclusions detected via backscattered electron imaging. Only inclusion-free amphibole crystals were analyzed. Sector zoning of the amphiboles is evident only in the experiments on starting material T85.

When present, the plagioclase crystals are small (5–10 microns) and often fill spaces between amphibole crystals. Fe–Ti oxides are present in most charges, but are most abundant in the alkali-rich starting compositions. The oxides form euhedral crystals and are dispersed throughout the charge. In the vast majority of the experiments, the equilibrium oxide is magnetite. Separate analysis of these oxides (Nielsen et al., in press) indicates that they have low partition coefficients for the REE and the HFSE. Therefore, any quench crystallization related to them will have relatively minor effects on the HFSE content of the melt.

The amount of melt in the experiments ranges from 20% in some of the 2 kbar, 900°C experiments, to >60% in some 5 kbar, 940°C runs. In most, interstitial melt percentages average between 20–40% (Table 2). Glass is clear, and quench crystallization is minor. The melt compositions range from dacite to tonolite to rhyolite, with generally low MgO (Table 2).

The IHPV experiments run under reducing conditions contain the same phases as the more oxidized experiments, except that the oxide phase is ilmenite rather than magnetite. However, for a given temperature and starting composition, glass is considerably less abundant in the reduced experiments. A series of piston cylinder experiments were run on undoped powders of the same starting compositions as part of a different study (f_{O2} 1–2 log units below QFM; Patinõ-Douce and Beard, 1995). Those experiments did not yield significant amounts of glass under the same conditions as used for this study. That

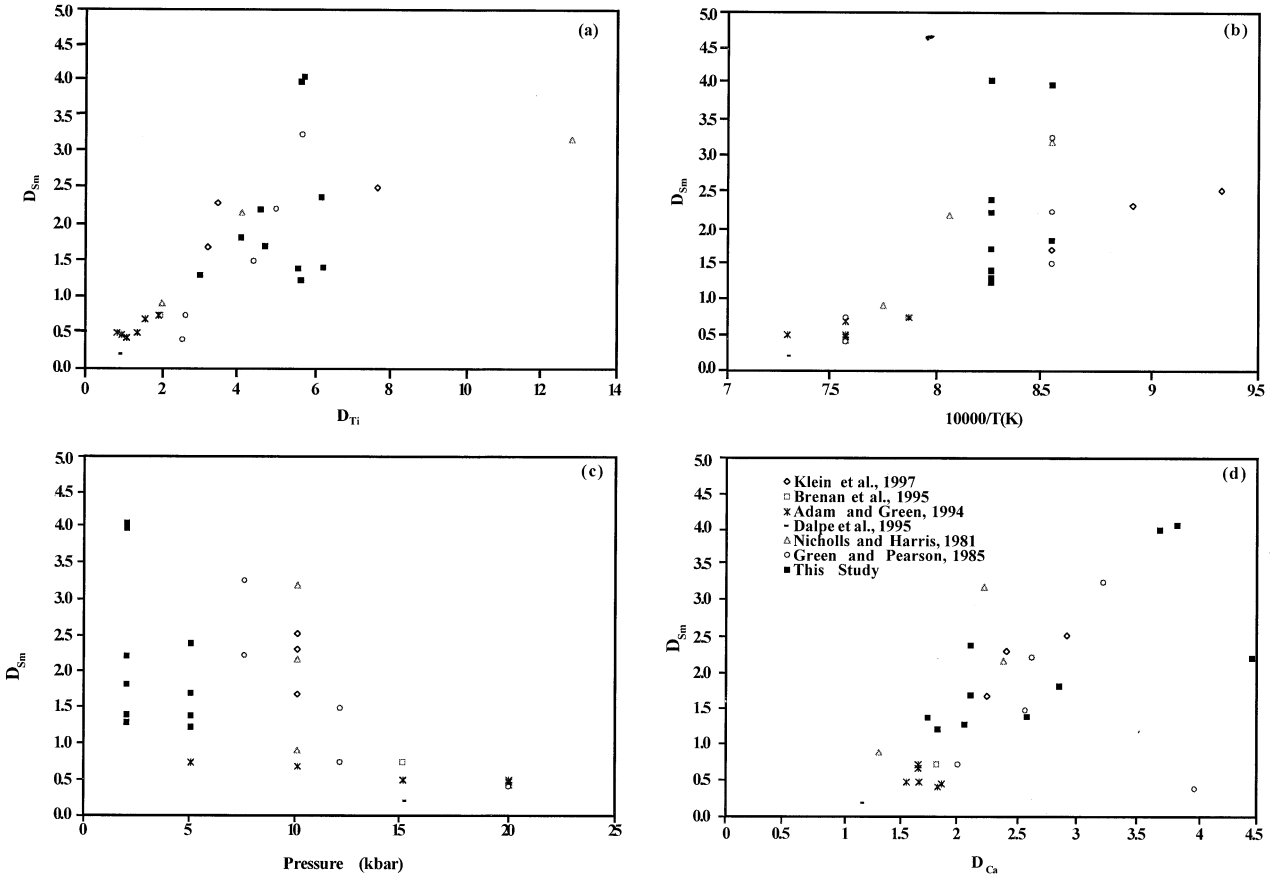

Fig. 1. Trace element vs. temperature for D_{Sm} for data from this investigation and from the literature (Nicholls and Harris, 1980; Green and Pearson, 1985; Adam and Green, 1994; Brenan et al., 1995; Dalpe et al., 1995; Klein et al., 1997). Data encompasses compositional ranges from basalt to low-Si rhyolite, temperatures of 900°C–1000°C, and pressures of 2–20kb.

effect may be due to the dopant, however given the high partition coefficients for these elements, it is unlikely that their addition will substantially lower the solidus. As an alternative explanation, we speculate that oxidizing conditions enhance the stability of magnetite. This may result in a more siliceous melt and consequently more melt at a given temperature due to the lower bulk partition coefficent for Si for the more oxidized experiments caused by an increase in the fraction of magnetite in the crystallizing mineral proportions.

Amphiboles range in composition from edenite through pargasitic hornblende to ferroan pargasite. Because the amphiboles in these experiments did not equilibrate under the same conditions as did the rocks that made up the starting composition, direct comparison is not possible. However, comparison with the results on undoped experiments indicates that the amphibole and melt compositions are not significantly different (see Beard and Lofgren, 1991), with the majority in both cases being "normal" pargasitic amphibole.

The homogeneity of the amphibole and glass was quantitatively evaluated by dividing the standard deviation of each analysis by the counting statistics calculated on an individual measurement (R_h—LaTourrette et al., 1995). This ratio gives a measure of the average deviation from the mean, in units of 1σ counting errors. A value of $R_h \leq 2$ means that the data lie within 2σ of the mean, which designates acceptable analytical homogeneity (LaTourrette et al., 1995). With the exception of La, Nb, and Ti for some charges, all the R_h values for our experiments are less than 2. Those samples with the greatest R_h values for Ti are the T85 starting materials, consistent with minor sector zoning in the amphibole. Sector zoning is characteristic of the pyroxene phenocrysts in the source rock (Duncan et al., 1995), and from the experiments on pyroxene partitioning for this same starting composition (Forsythe et al., 1994; Hack et al., 1994).

The count rates for the doped elements are on the order of 300–500 cts/sec/wt% (net peak), with a peak to background ratio of ~7 at 1 wt%. For counting times of 60–300 seconds, over 50000 counts (net peak) were collected for each analysis. Nevertheless, the relatively high La and Nb R_h can be attributed to the low concentrations, and therefore net counts for La and Nb in the amphiboles, significantly below the levels for which Rh is a valid measure. The 2σ standard deviation of each of the trace elements ranges between 0.01 and 0.23 wt.%, generally representing less than 10–15% relative variation. The degree of inter-crystalline and melt homogeneity indicates that the amphibole crystals grew in a well-mixed melt, and that no significant chemical boundary layers existed around the growing crystals.

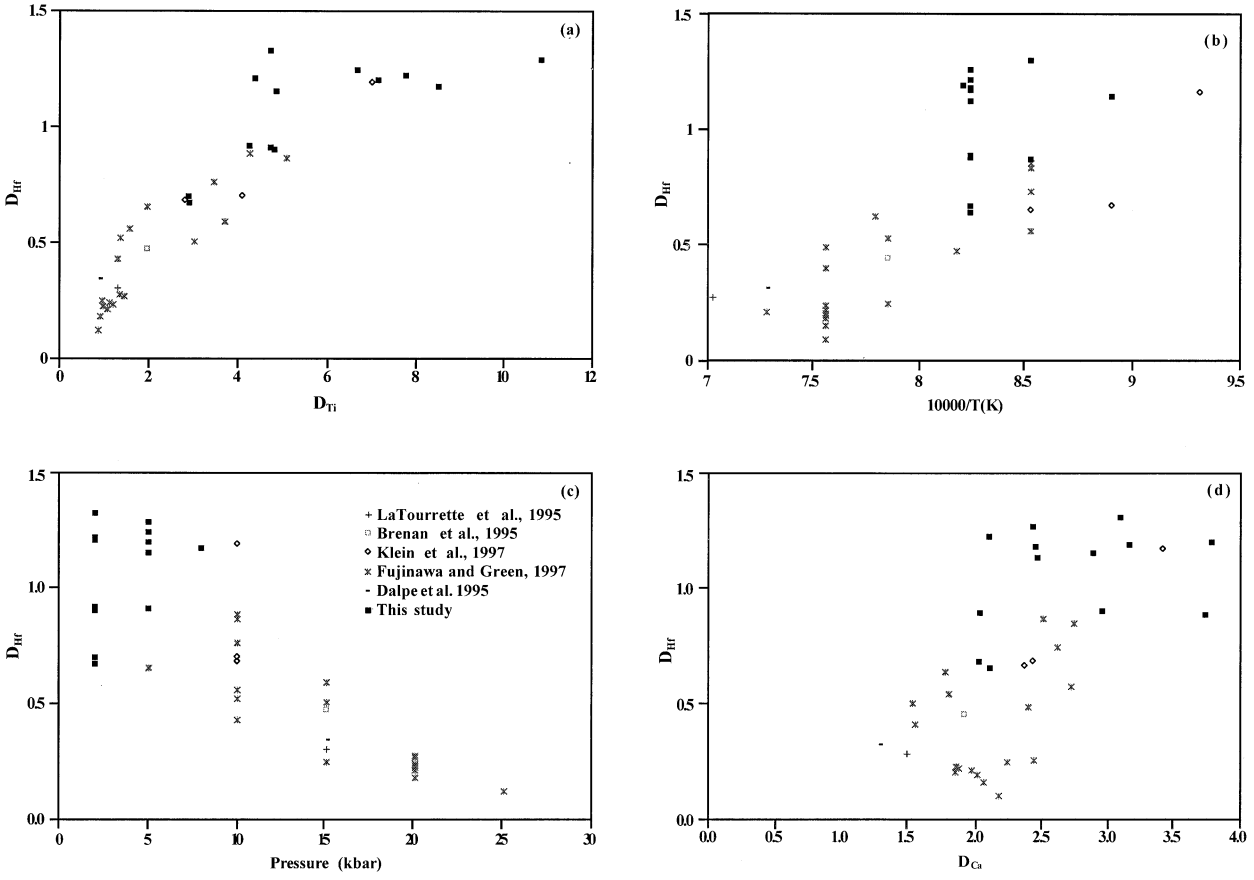

Fig. 2. Trace element vs. temperature for D_{Hf} for data from this investigation and from the literature (Brenan et al., 1995; Dalpe et al., 1995; LaTourrette et al., 1995; Fujinawa and Green, 1997; Klein et al., 1997). Data encompasses compositional ranges from basalt to low-Si rhyolite, temperatures of 900°C–1000°C, and pressures of 2–20kb.

To identify the important parameters that control partitioning of trace elements into amphibole, we compared the partition coefficients to single parameters, keeping in mind that a number of parameters may be involved. This methodology proved successful in the analysis of partitioning in pyroxenes and oxides (Gallahan and Nielsen, 1992; Hack et al., 1994; Forsythe et al., 1994), where correlations between D_{REE*} and D_{HFSE*} with Al in melt, and Ca in the pyroxene were detected, and used to parameterize expressions that quantified partitioning.

When the data set for amphibole was examined, a variety of parameters exhibited correlation with D_{REE*} and D_{HFSE*} (Fig. 1, 2). However, those correlations were not tight, exhibiting a wide range of values at any specific value of the correlated parameter. If we examine two examples, Sm from the REE group and Hf from the HFSE group, we can see that both decrease with increasing pressure and temperature. However, this can be somewhat misleading in that the compositions of the experimental systems are also correlated with pressure and temperature. For example, for rational geologic reasons, no one has done experiments on rhyolite at 20 kbar. All experiments above 10 kbar and 950°C are on basaltic compositions. The range of values at low temperature and pressure are necessarily wider due to the greater diversity of magma compositions in the crust. D_{REE*} correlates relatively well with D_{Ca*} and D_{Ti*}, however, there is significant variability in D_{Sm*} at any D_{Ca*} and D_{Ti*}. For D_{HFSE*}, there is essentially no correlation with D_{Ca*}, but there is a coherent relationship (but not necessarily linear) with D_{Ti}. This supports the contention that Ti and the HFSE occupy the C (M2) sites, and the REE occupy the B (M4) sites with Ca. This decoupling of the behavior of the REE and HFSE is significantly different from what has been observed for clinopyroxene (Forsythe et al., 1994; Hack et al., 1994).

The patterns of trace element behavior obtained from this study are similar in form to those found in previous investigations described above (Nicholls and Harris, 1980; Green and Pearson, 1985b; Adam et al., 1993; Adam and Green, 1994). The typical amphibole patterns show a slight depletion in the LREE's, a maximum at Ho and a slight decrease in D_{HFSE*} (Table 3). The range of D_{HFSE} is relatively narrow, with $D_{HF*} > D_{Zr*} > D_{Ta*} > D_{Nb*}$. The full range of values is less than 25% of that exhibited for clinopyroxene (Forsythe et al., 1994; Hack et al., 1994).

8. DISCUSSION

8.1. Application of Constraints

As noted above, the partitioning of the REE and Sc, Ti, V, Cr, Sr, Y, and Zr between amphibole and melt has been found

Table 3. Partition coefficients determined in this study. D-values were calculated from cation normalized mole fractions. LLH–La, Lu, Hf; NST–Nb, Sm, Ta; YZG–Y, Gd, Zr. The error measure presented is the standard deviation of multiple determinations of the composition of local mineral-melt pairs.

Exper.	P (kbar)	T(°C)	D_{Ti}	2σ	D_{La}	2σ	D_{Lu}	2σ	D_{Hf}	2σ
T85LLH	5	940	10.84	2.46	0.27	0.07	1.55	0.31	1.19	0.11
ABALLH	5	940	6.68	1.39	0.16	0.06	1.24	0.20	0.90	0.23
478LLH	5	940	4.73	1.23	0.16	0.05	1.25	0.22	0.76	0.18
AT4LLH	5	940	7.14	1.66	0.28	0.07	1.72	0.22	1.07	0.11
557LLH	5	940	4.85	1.46	0.40	0.05	1.97	0.17	1.02	0.21
T85LLH	2	945	7.77	1.61	0.64	0.24	2.17	0.25	1.87	0.20
T85LLH	2	940	4.38	0.98	0.20	0.04	0.98	0.23	1.00	0.22
ABALLH	2	940	4.25	0.67	0.18	0.04	1.44	0.27	0.77	0.22
478LLH	2	940	2.90	0.37	0.10	0.01	1.86	0.15	0.45	0.09
557LLH	2	940	2.89	0.66	0.35	0.07	2.52	0.17	1.45	0.16
478LLH	2	900	4.73	0.75	0.36	0.08	2.03	0.14	1.31	0.18
557LLH	2	900	4.80	0.80	0.25	0.06	2.22	0.24	0.98	0.15
	P (kbar)	T(°C)	D_{Ti}	2σ	D_{Nb}	2σ	D_{Sm}	2σ	D_{Ta}	2σ
T85NST	5	940	13.19	2.29	0.69	0.18	3.20	1.04	1.00	0.07
ABANST	5	940	5.42	0.95	0.20	0.03	1.21	0.24	0.23	0.06
478NST	5	940	5.61	1.28	0.52	0.16	2.27	0.57	0.57	0.14
AT4NST	5	940	5.23	1.59	0.24	0.04	1.32	0.37	0.27	0.09
557NST	5	940	4.40	0.46	0.28	0.09	1.63	0.26	0.30	0.12
T85NST	2	945	6.04	1.38	1.00	0.19	3.58	0.90	1.60	0.24
T85NST	2	940	4.13	1.47	0.73	0.17	2.00	0.33	0.54	0.11
478NST	2	940	2.81	0.65	0.28	0.06	1.25	0.28	0.17	0.07
AT4NST	2	940	5.67	1.53	0.49	0.12	1.32	0.31	0.49	0.11
557NST	2	940	5.12	0.82	0.69	0.18	2.93	0.40	0.80	0.18
478NST	2	900	3.92	0.76	0.65	0.15	1.77	0.28	0.72	0.09
557NST	2	900	5.27	0.87	0.63	0.12	3.07	0.54	0.76	0.17
	P (kbar)	T(°C)	D_{Ti}	2σ	D_{Y}	2σ	D_{Zr}	2σ	D_{Gd}	2σ
ABAYZG	5	940	6.62	2.70	1.65	0.31	0.68	0.07	2.07	0.24
478YZG	5	940	6.00	2.63	1.81	0.24	0.67	0.19	2.41	0.34
AT4YZG	5	940	6.33	1.96	1.62	0.25	0.81	0.15	2.10	0.12
557YZG	5	940	5.16	1.23	2.53	0.33	0.75	0.13	3.29	0.26
T85YZG	5	940	11.44	1.96	2.83	0.25	1.06	0.16	4.00	0.70
T85YZG	2	945	5.67	1.75	1.30	0.14	0.94	0.20	2.20	0.52
T85YZG	2	940	4.73	0.34	1.58	0.11	0.59	0.27	2.00	0.08
478YZG	2	940	3.36	0.68	2.07	0.11	0.25	0.06	2.05	0.22
AT4YZG	2	940	3.52	0.89	1.95	0.24	0.27	0.06	2.08	0.07
478YZG	2	900	3.94	0.78	3.10	0.32	0.77	0.17	2.79	0.15
557YZG	2	900	2.75	0.41	1.62	0.23	0.29	0.05	2.00	0.17

to be variably correlated to D_{Ca} (Sisson, 1994), similar to the relationship noted for clinopyroxene discovered by McKay et al. (1986). The data obtained in this, as well as, previous studies were used to predict REE partitioning using both the parameters obtained by Sisson (1994), and parameters obtained by regressing our data to D_{Ca}. Results using the Sisson (1994) parameters overestimate the partitioning of trace elements for basaltic systems (Fig. 3). We attribute the anomalous values for basaltic systems to the fact that the Sisson (1994) constants were regressed against silicic systems only. Regression of our data set against D_{Ca} alone resulted in low R^2 values (0.2–0.3), consistent with the lack of correlation with Ca, particularly for the HFSE, indicating that additional parameters are needed to accurately describe the partitioning of trace elements over a wide range of compositions and conditions.

The effects of physio-chemical properties of the amphibole crystal were modeled after the method of Blundy and Wood (1994) and Wood and Blundy (1997). The data define several parabolas (Onuma curves) when plotted as a function of partitioning against ionic radii (Fig. 4). Values of D_o, r_o, and E were obtained from a least squares best fit through the data. These constants were used to calculate curves describing the partition coefficient as a function of ionic radius. However, the application of these expressions is handicapped by the same lack of strong correlation with Ca partitioning that was found for the Sisson (1994) approach.

Therefore, it is evident that more parameters need to be included in the model if we are to quantify REE and HFSE for a wide range of liquid compositions. The effects of changing melt component activities may be modeled by utilizing a correlation with the behavior of a known element (e.g., D_{Ca}), or by the application of a melt component activity model. The pressure and temperature effects on crystal structure can be modeled as a function of crystal strain. Yet, these models do not fully incorporate the effects of changing melt component activities, substitution mechanisms, and changing physical parameters of the crystal structure. It is evident that the partitioning of REE and HFSE in amphibole can be correlated both to

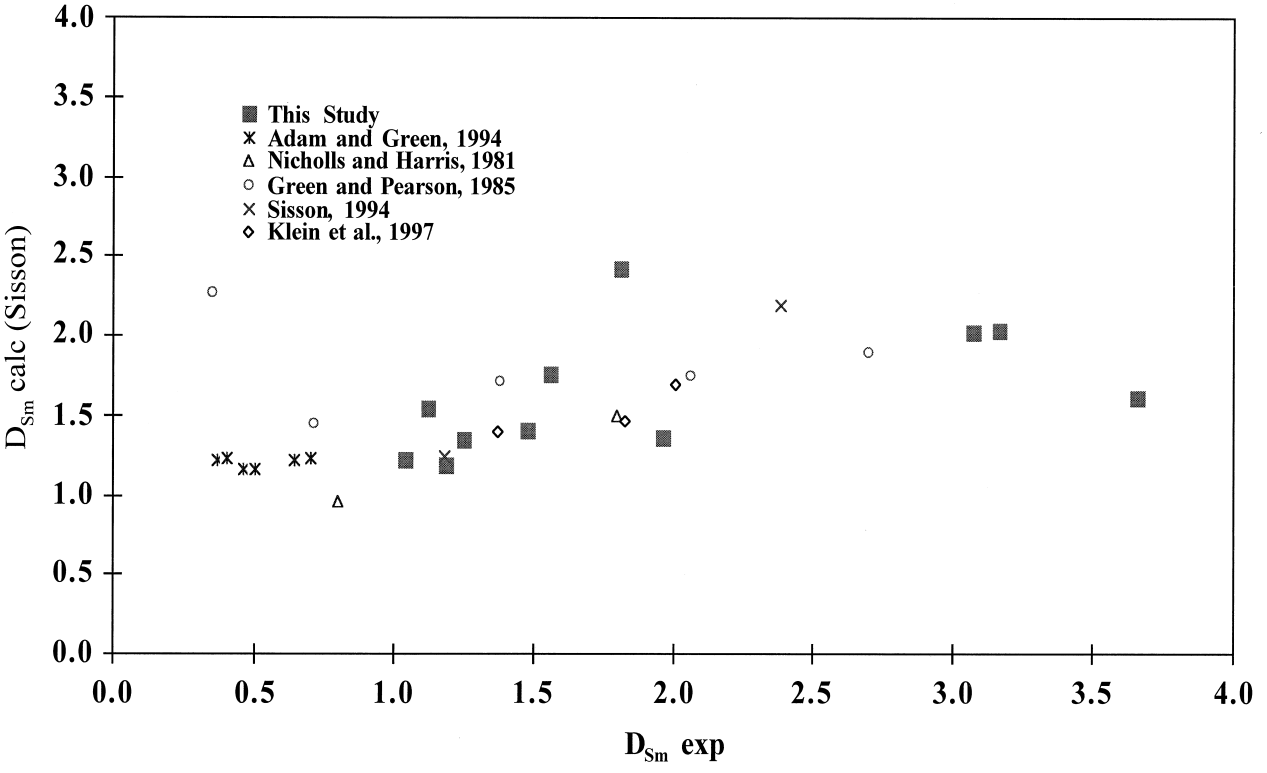

Fig. 3. Application of regressions derived in Sisson (1994) to basaltic to dacitic composition systems. Note that the data significantly departs from the regression for basaltic compositions.

mineral and to melt components. The observed correlations with the behavior of Ti, Al, Si, Ca, temperature and pressure are not surprising in that these are the critical components in expressions of amphibole-melt equilibria. However, if we are to produce numerical means for predicting partitioning behavior in natural systems, we must decide from a pragmatic standpoint how to calculate expressions that include the important controls, yet are usable, even when we do not know the activity coefficients, the identity, nor the relative importance, of the trace element substitution mechanisms.

Our approach applies the use of multiple regressions on linked, compensated partition coefficients, the selection of which is based on the observed correlations, and the robustness of the results. Specifically, we consider the equilibrium constant for a potential Zr amphibole formation reaction (Eqn. 2 above) in terms of compositionally compensated partition coefficients, assuming the validity of the two-lattice melt model as a first approximation:

$$\ln(d^*_{Zr}\, d^*_{Na}\, d^{*4}_{Mg}\, d^{*2}_{Ca}\, d^{*3}_{Al}\, d^{*5}_{Si}) = -\Delta H/RT + P\Delta V/RT + \Delta S/R \quad (7)$$

where ln is natural log, H is enthaphy, T is temperature in Kelvin, P is pressure, V is volume and S is entropy. Converting $\Delta H/R$, ΔV, ΔS, and the variable stoichiometry for each component to constants, and rearranging to solve for $\ln d^*_{Zr}$ yields:

$$\ln d^*_{Zr} = A\ln d^*_{Na} + B\ln d^*_{Mg} + C\ln d^*_{Ca} + D\ln d^*_{Al} + E\ln d^*_{Si} + F/T + GP + H \quad (8)$$

The constants A–E combine the stoichiometry of the reaction and the error related to the assumptions of the mixing properties of the components. These constants can be calculated by multiple linear regression and used to predict trace element partitioning in systems where all the terms (mole fractions, T and P) are known.

We tested different combinations of parameters, measuring their success in terms of R^2 of the regression, and the precision with which they reproduced the input data set. That data set was made up of all the existing published data, plus the results of this study. Over 100 different combinations of parameters were applied, resulting in a set of expressions (Table 4) that reproduce the input data set partition coefficients within 15–33 %. The partition coefficients in the data set range over an order of magnitude (e.g., 0.2–2.0) or more. Therefore, the errors represent ~5–15% of the total range. This error is up to twice the normally cited analytical and experimental error of the data (~5–10% relative). A sample calculation demonstrates the intermediate steps in the calculation of D from a mineral and melt composition (Table 5).

The highest R^2 obtained was for expressions including terms for the compensated partition coefficients for Ca, Al, Si, Ti, the Fe–Mg exchange reaction, temperature and pressure. An additional empirical alkalinity term (Na + K/Al) improved the fit for the REE in the alkaline experiments (e.g., T85). The use of compensated partition coefficients for Na and K components did not result in improved fits. We attribute this to the difficulty in obtaining accurate alkali compositions for hydrous, silicic

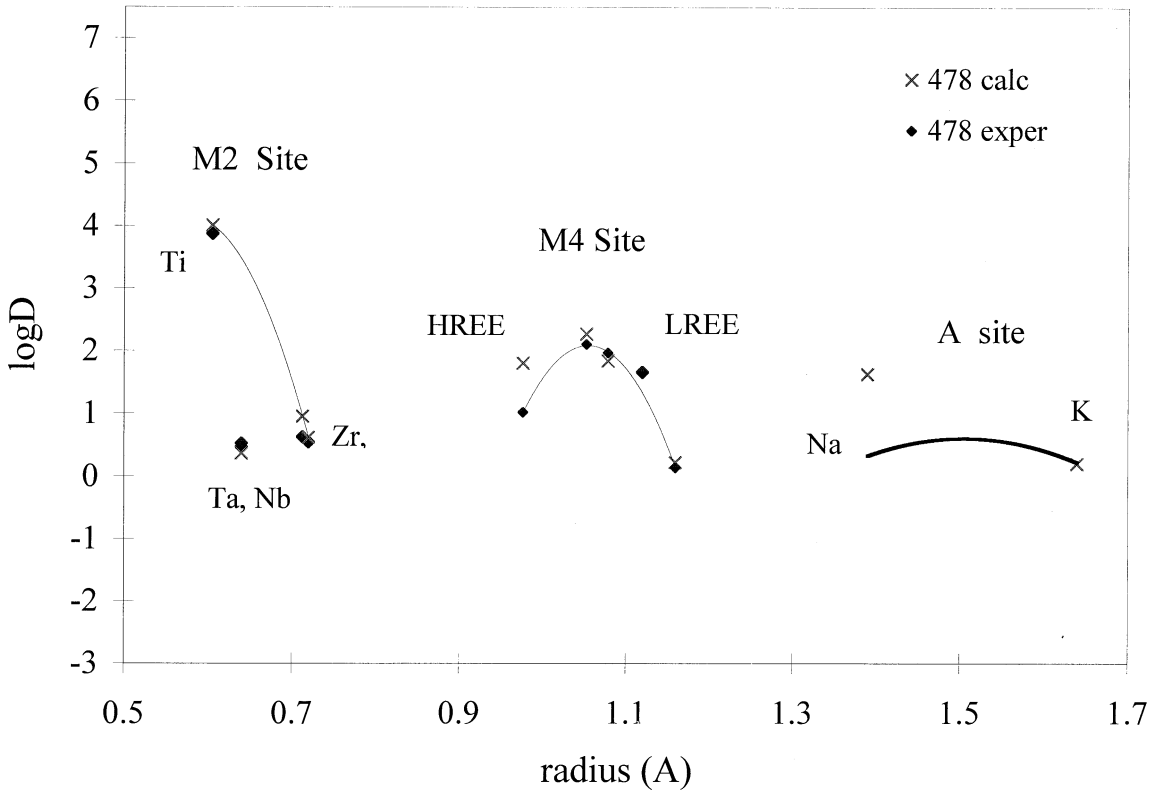

Fig. 4. Trace element partition coefficients plotted as a function of radius (after LaTourrette et al., 1995). Values form a parabola who's maxima defines the ideal ionic radius (r_o) and optimal partition coefficient (D_o). E is a function of the half-width of the parabola. Solid diamonds–measured partition coefficients, X's–partition coefficients predicted on the basis of crystal strain.

glasses. Expressions excluding pressure and temperature resulted in only a minor decrease in R^2 (Table 4). We attribute this to the fact that the compositional components are themselves dependent on temperature. These latter expressions require only information obtainable from standard electron microprobe analysis.

Table 4. Constants for multiple linear regressions describing the relationship between the natural log of d* for the trace elements of interest, and temperature, pressure and phase composition. These expressions are available in the form of a spreadsheet or program from either the author or from the trace element section of the GERM web site (http://www.ep.es.llnl.gov/germ). Mg ex is the Fe–Mg exchange reaction (e.g. D_{Fe}/D_{Mg}). Alkalinity–molar (Na+K)/Al. d* compensated partition coefficient. IP–internal precision calculated as the 1σ standard deviation of 100* ($D_{calc} - D_{obs}$)/D_{obs}. Note that the full range of values for each data set covers 1000–2000% (factor of 10–20).

	Constant	10000/T (K)	P (kbar)	ln d^*_{Ti}	lnd^*_{Ca}	ln Mg ex	ln d^*_{Si}	ln d^*_{Al}	Alkalinity	R^2	IP
ln d^*_{Zr}	−5.510	0.321	−0.005	0.401	−0.248	−0.142	−0.350	0.237	−0.211	0.62	35
	−2.714			0.592	−0.479	−0.065	0.005	−0.011		0.60	37
ln d^*_{Nb}	−0.813	0.037	−0.014	1.290	1.496	0.517	−1.598	−0.131	0.828	0.96	15
	0.052			1.342	1.252	0.388	0.301	0.052		0.93	18
ln d^*_{La}	−1.958	0.320	−0.016	0.229	3.534	−0.187	2.281	1.221	−2.337	0.80	32
	−0.728			0.537	1.456	0.031	1.418	−0.135		0.65	34
ln d^*_{Sm}	−0.841	0.250	−0.006	0.544	0.598	0.075	2.233	−0.163	−0.109	0.88	24
	0.860			0.779	0.607	0.138	2.025	−0.375		0.88	28
ln d^*_{Gd}	−1.250	0.170	0.017	0.430	0.571	0.141	2.265	0.080	−1.277	0.98	15
	1.300			0.653	0.747	0.097	2.086	−0.503		0.93	19
ln d^*_{Y}	−2.331	0.424	0.002	0.574	0.777	0.049	1.793	0.176	−0.484	0.81	27
	0.784			0.690	0.467	0.133	1.601	−0.405		0.78	33
ln d^*_{Lu}	−2.033	0.422	−0.005	0.424	0.628	0.198	3.944	0.274	−1.288	0.95	17
	0.490			0.606	0.400	0.070	2.076	−0.472		0.88	22
ln d^*_{Hf}	−0.049	0.003	−0.057	0.928	2.326	−0.198	−0.719	1.237	−1.824	0.77	28
	−2.152			1.218	0.492	−0.290	−1.279	−0.068		0.68	32
ln d^*_{Ta}	1.197	−0.151	−0.001	1.701	1.340	0.633	−1.465	0.068	0.659	0.93	24
	0.207			1.570	1.248	0.458	−0.277	0.330		0.92	27

Table 5. Sample calculation for La partitioning using the results from T85LLH experiment run at 5 kbar, 940°C.

	Amphibole	Mol. wt.	Cation propor.	Cation mol. frac	Glass	Cation propor.	Cation mol. frac	Two lattice activity	Regression parameters	Regression constants	Value calc. from exper.
SiO_2	40.13	60.08	0.668	0.3798	60.23	1.0025	0.4856	0.8481	ln d^*_{Ti}	0.229	0.620
TiO_2	3.53	79.90	0.044	0.0251	0.34	0.0043	0.0021	0.0135	ln d^*_{Ca}	3.534	−0.943
Al_2O_3	14.23	51.00	0.279	0.1586	18.56	0.3639	0.1763	0.5853	10000/T(K)	0.320	8.244
FeO	11.44	71.84	0.159	0.0905	1.17	0.0163	0.0079	0.0517	ln Mg*	−0.187	3.748
MnO	0.19	70.94	0.003	0.0015	0.11	0.0016	0.0008	0.0049	ln d^*_{Si}	2.281	−0.803
MgO	12.45	43.00	0.290	0.1646	0.03	0.0007	0.0003	0.0022	ln d^*_{Al}	1.221	−1.305
CaO	11.99	56.08	0.214	0.1216	5.51	0.0983	0.0476	0.3120	ln alkalinity	−2.337	−1.559
K_2O	1.35	47.10	0.029	0.0163	0.83	0.0176	0.0085	0.0149	Pressure	−0.016	5
Na_2O	2.18	30.99	0.070	0.0400	5.02	0.1620	0.0785	0.1370		−1.958	
P_2O_5	0.00	70.97	0.000	0.0000	0.33	0.0046	0.0023	0.0148		sum NM	0.1525
La_2O_3	0.12	162.91	0.001	0.0004	0.46	0.0028	0.0014	0.0090		SUM NF	0.5726
Lu_2O_3	0.23	198.97	0.001	0.0007	0.15	0.0008	0.0004	0.0024		D_{La} calc	0.30
HfO_2	0.32	210.49	0.002	0.0009	0.28	0.0013	0.0006	0.0042		D_{La} obs	0.27
H_2O	Σ		1.759	1.0000	6.98	0.3878	0.1878				
						2.064406	1				

Cation proportions are the oxide wt.% divided by the molecular wt. The cation mole fractions equal the cation proportions normalized to one. The two lattice activity equals the cation normalized mole fraction divided by the sum of the mole fractions of the cations in the network formers or network modifiers. For example, the activity of Al equals the mole fraction of Al minus Na and K divided by the sum of Ti, Al, Fe, Mn, Mg, Ca, P, La, Lu, Hf minus K and Na. Mg* is the Mg–Fe exchange reaction, equal to D_{Mg}/D_{Fe}. The regression constants are from Table 4. ln d^*_{La} is calculated by summing the product of the regression constants and the values calculated from the experiment. D_{La} can be determined by taking the exponent of lnd*La and dividing by the sum of the network modifiers. The expressions derived here, and sample calculations are available from the first author in spreadsheet form. In addition, they are available to download from the GERM website (www-ep.llnl.gov/germ).

We found that we obtained higher R^2 using compensated partition coefficients (d* terms) rather than simple partition coefficients or compositional parameters (e.g., Ca content of the amphibole). This correlation with d^*_{Ca}, as opposed to the Ca content of the amphibole illustrates the advantage of a model that includes the effects of melt composition as an explicit parameter.

The minimum requirement for these expressions is that they accurately reproduce the calibration data set (Fig. 5) and should exhibit little systematic variability as a function of composition. These expressions satisfy both criteria, with only minor departures exhibited by the more alkaline compositions. A potential problem with these constraints is caused by the fact that the number of experimental runs, and experimental compositions is different for each element. This difference may be exhibited in the regression parameters, generating unrealistic REE patterns when applied to magmas outside the calibration data set. To test for this, we calculated REE patterns from the liquid compositions from the Hf partitioning experiments**.** None of these experiments were doped with the full range of REE, but they represent a wide range of magma types and compositions (alkali basalt to rhyolite). The generated patterns are generally smooth, and reproduce the shape of the normal amphibole distribution, with the high at ~Dy–Ho (Fig. 6).

Since no data from high Si rhyolitic compositions were included in the calibrating data set, extrapolation of these regressions into high silica systems is not recommended. Within that constraint, however, these models have important, practical implications for calculation and use of amphibole-melt partition coefficients in natural systems. The parameters required for the model (d^*_{Ti}, d^*_{Ca}, d^*_{Al}, d^*_{Si}, Mg/Fe exchange) are readily obtained from standard microprobe analyses.

8.2. Prediction of Ti Content in Amphibole

The correlation of D_{REE*} and D_{HFSE*} with D_{Ti*} and its relative importance in the regressions, indicates that the partitioning of REE and HFSE into amphibole may be approximated by the behavior of Ti over a wide range of conditions. This same correlation has been observed in pyroxenes and magnetite (Gallaghan and Nielsen, 1992; Forsythe et al., 1994; Nielsen et al., 1994; Nielsen et al., in press). However, since the Ti content is not always known, it is useful to be able to predict the partitioning behavior of Ti over as wide a range of compositions as possible.

Factor analysis of the Ti data indicates that the partitioning of Ti can be described by the same parameters as other HFSE (Ca, Si, Al, Mg–Fe exchange). Regression constants and parameters that describe the partitioning of Ti into amphibole are:

$$\ln d^*_{Ti} = 4970/T(K) - 0.047P(kb) + 0.13\ln d^*_{Ca} + 0.433\ln d^*_{Al} - 3.47\ln d^*_{Si} - 0.178\ln \text{Mg–Fe}_{exch} - 0.2252\ln(Na + K/Al) - 6.97 \quad (9)$$

Ti is inversely correlated to Mg–Fe exchange, indicating that Ti is controlled via a coupled substitution with Mg. This expression has an R^2 of 0.73, and reproduced the calibration data set with a 1σ internal precision of 27% (Fig. 5d).

8.3. Implications of REE and HFSE Partitioning in Amphibole

The partition coefficients determined in this study were used to model the hydrous partial melting of a hypothetical amphibolite. Starting mineral modes (45% plagioclase, 40% amphibole, and 12% quartz) were modified from the subsolidus composition 478 from Beard and Lofgren (1991). In order to illustrate what the relative effect of melting an amphibole has

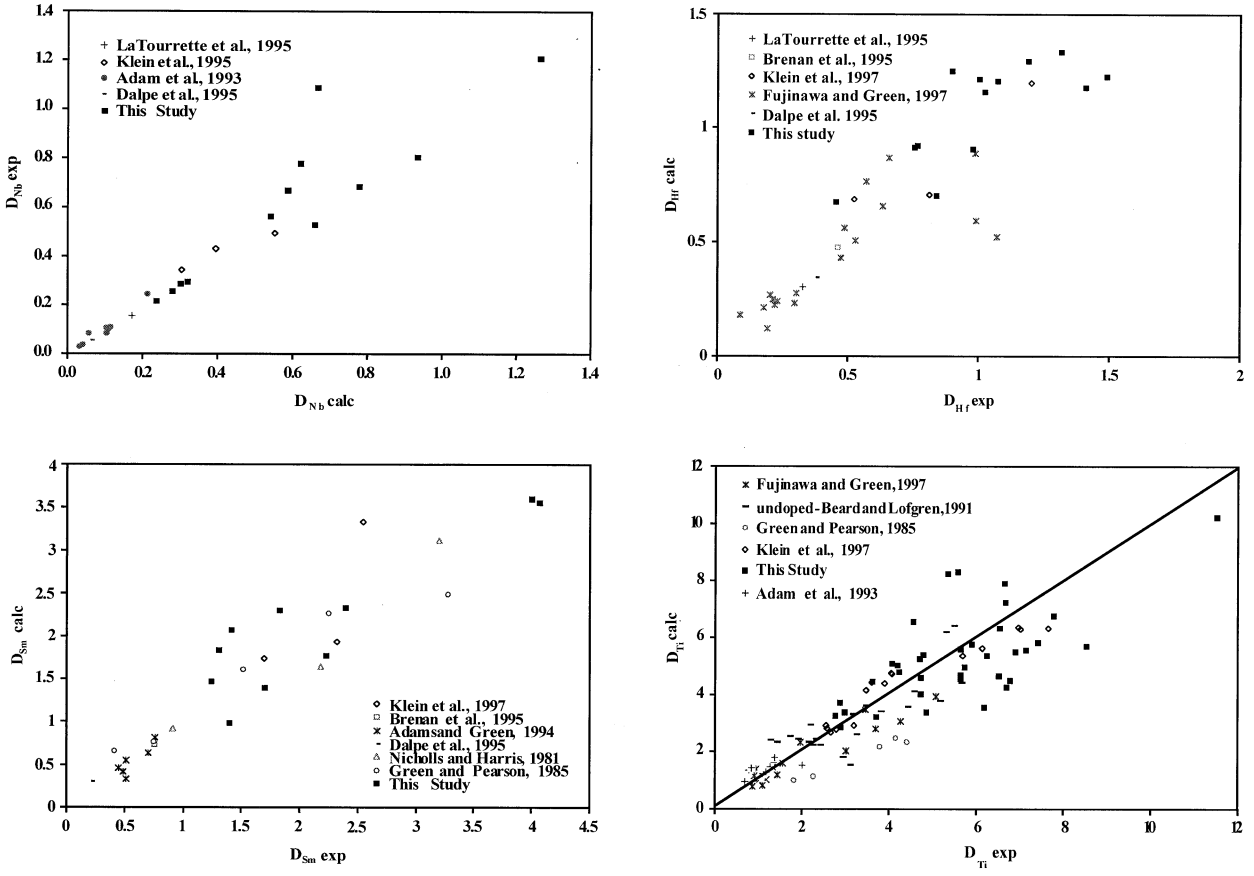

Fig. 5. Test of internal precision of multiple linear regressions for Ti, Nb, Hf and Sm that include temperature, pressure, and compensated partition coefficients for Si, Al, Ca, Ti and the Mg-Fe exchange reaction.

on the trace element chemistry, an initial concentration of 1 was chosen for all trace elements. We used a modal melting model in order to maximize the potential effects of amphibole. Even so, while fractional melting appears to deplete the melt in HFSE faster then does equilibrium melting, the relative shape of the trace element pattern is the same for both processes (Fig. 7a,b). The REE's in the melt show a typical convex down pattern, with a minimum at the middle REE's. In addition, partial melts have La/Lu ratios (2.0–7.0) similar to those observed in naturally occurring dacites (Romick et al., 1996).

Both fractional and equilibrium crystallization curves were calculated to assess the effect of amphibole fractionation on the trace element chemistry of a crystallizing magma (Figure 7c,d). The fractionating mode used (60% plagioclase, 31% amphibole, 9% magnetite) is similar to that used to model the Aleutian hornblende dacites (Romick et al., 1992). Melts generated by fractional crystallization of amphibole have relatively flat trace element patterns, with the exception of Ti. In addition, these melts are characterized by lower La/Lu ratios than those produced by partial melting. With the exception of Ti, there is no significant depletion of HFSE's within the partial melting or fractional crystallization melts, indicating that amphibole fractionation (or melting) alone cannot explain the HFSE depletion characteristic of calc-alkaline magmatism.

9. CONCLUSIONS

Partition coefficients for La, Sm, Gd, Lu, Ti, Zr, Hf, Ta, Nb between pargasitic amphibole and dacitic melts have been experimentally determined for pressures of 2 and 5 kb and temperatures of 900°C to 945°C. The shape of the D-value patterns are similar to those determined for basaltic systems, yet are systematically higher. The REE patterns for amphibole are convex, with a maximum at Ho. With the exception of Ti, D_{HFSE*} for amphibole are relatively similar.

The data from this study were combined with data obtained from previous studies to calibrate expressions that predict the partition coefficients for REE and HFSE into amphibole in basaltic to low-Si rhyolite systems with internal precision of 15–35%. The fact that these expressions were derived from partitioning data obtained from basaltic to low Si rhyolite compositions, temperatures of 850°C to 1100°C, and pressures of 2–20 kbar, makes these regressions applicable to a wide range of geologic systems, including mid-ocean ridge, volcanic arc, and continental regimes. The expressions derived from this study should not be extrapolated to high silica systems, as no rhyolitic composition partitioning data was included in this study. However, the expressions derived here provide a useful means to predict amphibole-melt partition coefficients for REE

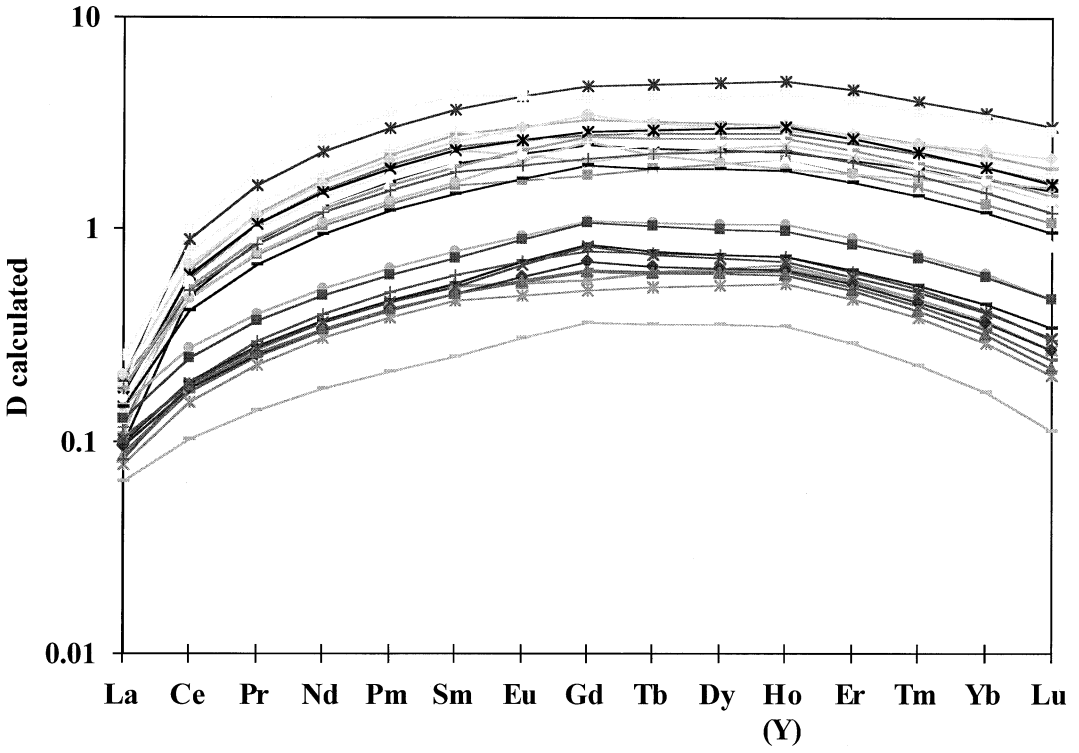

Fig. 6. Calculated REE patterns for liquids ranging from alkali basalt to low-Si rhyolite. Y is used as a proxy for Ho. La, Sm, Gd, Y and Lu were calculated, with the intervening elements extrapolated.

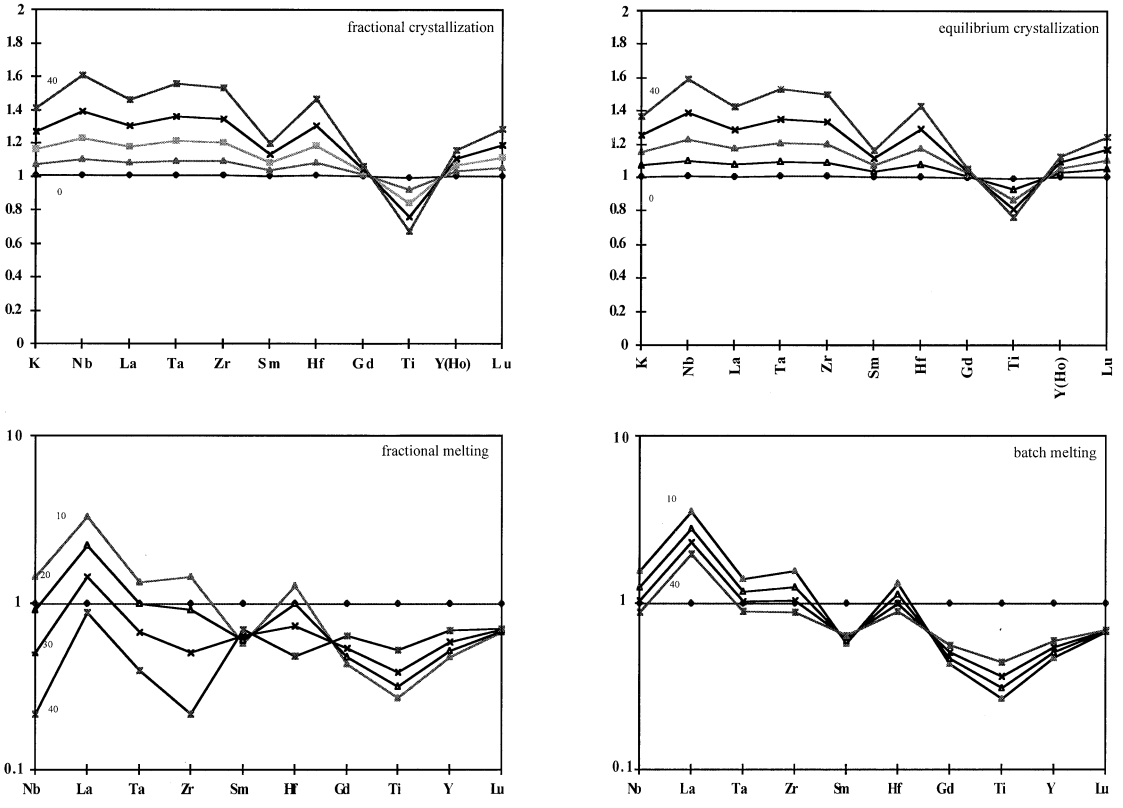

Fig. 7. Trace element patterns for a melt generated via (a) fractional melting; and (b) equilibrium melting of a hypothetical amphibolite. Modal proportions were modified from a subsolidus composition from Beard and Lofgren (1991). Curves represent calculations done at increments of 10% melting. Trace element patterns for a melt generated from (c) fractional and (d) equilibrium crystallization of modal proportions of 60% amphibole, 31% plagioclase, and 9% magnetite. Curves represent calculations done at increments of 10% crystallization of a dacitic parent magma.

and HFSE for which standard (e.g., microprobe) compositional data is available.

Fractional crystallization and partial melting calculations involving amphibole indicate that crystallization or melting of amphibole alone does not explain the HFSE depletion that is characteristic of arc magmas. However, the fact that REE patterns of amphibole bearing dacites are very similar in shape to that of amphibole underscores the importance of this mineral to the genesis of hydrous melts of intermediate composition.

Acknowledgments—We would like to thank Bob Bodnar at Virginia Polytechnic for providing access to his equipment, without which this project would have been impossible. Don Baker and two anonymous reviewers greatly improved the first version of this manuscript. This research was supported by NSF grant EAR9406134.

REFERENCES

Adam J. and Green T. H. (1994) The effects of pressure and temperature on the partitioning of Ti, and REE between amphibole, clinopyroxene, and basanitic melts. *Chem. Geol.* **117,** 219–233.

Adam J., Green T. H., and Sie S. H. (1993) Proton microprobe determined partitioning of Rb, Sr, Ba, Y, Zr, Nb, and Ta, between experimentally produced amphiboles and silicate melts with variable F content. *Chem. Geol.* **109,** 29–49.

Allen J. and Boettcher A. L. (1983) The stability of amphibole in andesite and basalt at high pressures. *Am. Mineral.* **68,** 219–233.

Anderson A. T. (1974) Before eruption H_2O content of some high alumina magmas. *Bull. Volc.* **37,** 530–52.

Beard J. S. and Lofgren G. E. (1991) Dehydration Melting and water-saturated melting of basaltic to andesitic greenstones and amphibolites at 1, 3, and 6.9 kb. *J. Petrol.* **32,** 365–401.

Beard J. S. (1986) Characteristic mineral of arc-related cumulate gabbros: Implications for the tectonic setting of gabbroic plutons and for andesite genesis. *Geology* **14,** 848–851.

Beattie P. (1994) Systematics and energetics of trace-element partitioning between olivine and silicate melts: Implications for the nature of mineral/melt partitioning. *Chem. Geol.* **117,** 57–71.

Beattie, P., Drake, M. J., Jones, J., Leeman, W., Longhi, J., McKay, G., Nielsen, R, Plame, H., Shaw, D., Takahashi, E., and Watson, B. (1993) Terminology for trace element partitioning. *Geochim. Cosmochim. Acta.* **57,** 1605–1606.

Beattie P., Ford C., and Russell D. (1991) Partition coefficients for olivine-melt and orthopyroxene-melt systems. *Contrib. Mineral. Petrol.* **109,** 212–224.

Blundy J. and Wood B. J. (1991) Crystal-Chemical controls on the partitioning of Sr and Ba between plagioclase feldspar, silicate melts, and hydrothermal solutions. *Geochim. Cosmochim. Acta* **55,** 193–209.

Blundy J. and Wood B. J. (1994) Prediction of crystal-melt partition coefficients from elastic moduli. *Nature* **372,** 452–454.

Brenan J. M., Shaw H. F., Phinney D. L., and Ryerson F. J. (1995) Rutile–aqueous fluid partitioning of Nb, Ta, Hf, Zr, U and Th: Implications for high field strength element depletions in island arc basalts. *Earth Planet. Sci. Let.* **128,** 327–339.

Brice J. C. (1975) Some thermodynamic aspects of the growth of strained crystals. *J. Crystal Growth* **28,** 249–253.

Castro A. and Edryd S. W. (1992) Amphibole-rich polycrystalline clots in calc-alkaline granitic rocks and their enclaves. *Can. Mineral.* **30, 4,** 1093–1112.

Cawthorn R. G. and O'Hara M. J. (1976) Amphibole fractionation in calc-alkaline magma genesis. *Am. J. Sci.* **276,** 309–329.

Comodi P., Mellini M., Ungaretti L., and Zanazzi P. F. (1991) Compressibility and high pressure refinement of tremolite, pargasite, and glaucophane, *Eur. J. Mineral.* **3,** 485–499.

Conrad W. C. and Kay R. W. (1984) Ultramafic and mafic inclusions from Adak Island: Crystallization history and implications for the nature of primary magmas and crustal evolution of the Aleutian arc. *J. Petrol.* **25,** 88–125.

Dalpe C., Baker D. L., and Sutton S. R. (1992) Partition coefficient of Ti, Cr, Ga, Rb, Sr, Y, Nb, and Zr between pargasite and nephelinic melt at 1.5 GPa, *EOS* **73,** 607 (abstr.).

Dalpe C. and Baker D.R. (1994) Partition coefficients for rare-earth elements between calcic amphibole and Ti-rich basanitic glass at 1.5 GPa, 1100°C. *Mineral. Mag.* **58A,** 207–208 (abstr.).

Dalpe C., Baker D. L., and Sutton S. R. (1995) Synchotron x-ray fluorescence and laser-ablation ICP-MS microprobes: Useful instruments for analysis of experimental run-products. *Can. Mineral.* **33,** 481–498.

Dautria J. M., Liotard J. M., Cabanes N., Girod M., and Briqueu L. (1987) Amphibole-rich xenoliths and host alkali basalts: Petrogenetic constraints and implications on the recent evolution of the upper mantle beneath Ahaggar (central Sahara, southern Algeria). *Contrib. Mineral. Petrol.* **95,** 133–144.

Deer W., Howie, R. A., and Zussman, J. (1992) *The rock forming minerals.* Addison Wesley Longman Ltd., 2nd edition.

Drake M. J. and Holloway J. R. (1981) Partitioning of Ni between olivine and silicate melt: The "Henry's Law problem" reexamined. *Geochim. Cosmochim. Acta* **45,** 431–437.

Drake M. J. and Weill D. F. (1972) New rare earth element standards for electron microprobe analysis. *Chem. Geol.* **10,** 179–181.

Drake M. J. and Weill D. F. (1975) The partition of Sr, Ba, Ca, Y, Eu^{2+}, Eu^{3+} and other REE between plagioclase feldspar and magmatic silicate liquid. *Geochim. Cosmochim. Acta* **39,** 689–712.

Duncan R. A., Fisk M. R., White W. M., and Nielsen R. L. (1995) Tahiti: Geochemical evolution of a French Polynesian Volcano. *J. Geophys. Res.* **99,** 24341–24357.

Ewart A. (1979) A review of the mineralogy and chemistry of Tertiary-recent dacitic, latitic, rhyolitic, and related sialic rocks: In *Trondhjemites, Dacites, and Related Rocks.* (ed. Barker, F.), pp. 13–112. Elsevier.

Ferreira V. P., Sial A. N., Fallick A. E., and Cruz M. J. M. (1995) Amphibole-rich clots in calc-alkalic granitoids and their mafic microgranular enclaves from two foldbelts, NE Brazil. U.S.G.S. Circular, pp. 49.

Foley S., Brumm R., Tiepolo M., Bottazzi P., Oberti R, Vannucci R., and Zanetti A. (1999) HFSE site preferences and coupled/decoupled behavior of Ti, (Nb, Ta) and (Zr, Hf) in amphiboles. *EOS* **80,** S360 (abstr.).

Forsythe L. M., Nielsen R. L., and Fisk M. R. (1994) The partitioning of HFSE between pyroxene and natural mafic to intermediate composition silicate liquids at 1 atm to 10 kb. *Chem. Geol.* **117,** 107–125.

Fujinawa A. and Green T. H. (1997) Experimental study of partitioning of Hf and Zr between amphibole, clinopyroxene and garnet and silicate melts. *Jap. J. Miner. Petrol. Econ. Geol.* **92,** 69–89.

Gallaghan W. E. and Nielsen R. L. (1992) Experimental determination of the partitioning of Sc, Y, and REE between high-Ca clinopyroxene and natural mafic liquids. *Geochim. Cosmochim. Acta* **49,** 1469–1468.

Garcia M. O., Liu N. W. K., and Muenow D. W. (1979) Volatiles in submarine volcanic rocks from the Marianas island arc and trough. *Geochim. Cosmochim. Acta* **43,** 305–312.

Ghiorso M. S. and Sack R. O. (1995) Chemical mass transfer in magmatic processes. IV. A revised and internally consistent thermodynamic model for the interpolation and extrapolation of liquid-solid equilibria in magmatic systems at elevated temperatures and pressures. *Contrib. Mineral. Petrol.* **119,** 197–212.

Goldschmidt V. M. (1937) The principles of distribution of chemical elements in minerals and rocks. *J. Chem. Soc. London* **655,** 655–673.

Green T. H. and Pearson N. J. (1985) Experimental determination of REE partition coefficients between amphibole and basaltic to andesitic liquids at high pressure. *Geochim. Cosmochim. Acta* **49,** 1465–1468.

Green T. H. (1994) Experimental studies of trace-element partitioning applicable to igneous petrogenesis—Sedona 16 years later. *Chem. Geol.* **117,** 1–36.

Hack P. J., Nielsen R. L., and Johnston A. D. (1994) Experimentally determined rare-earth element and Y partitioning behavior between clinopyroxene and basaltic liquids at pressures up to 20 kb. *Chem. Geol.* **117,** 89–105.

Hartel T. H. D. and Pattison D. R. M. (1996) Genesis of the Kapuskasing (Ontario) migmatitic granulites by dehydration melting of am-

phibolite: The importance of quartz to reaction progress. *J. Metamorph. Petrol.*, **14,** 591–611.
Hawthorne F. C. (1981) Crystal Chemistry of Amphiboles. In *Amphiboles and other hydrous pyriboles.* (eds. Veblen, D. R. and Ribbe, P. H.), *MSA Rev. Mineral.* **9a,** pp. 1–95.
Helz R. T. (1976) Phase relations of basalts in their melting ranges at P_{H2O} = 5 kb. Part II. Melt compositions. *J. Petrol.* **17,** 139–193**.**
Huang W. L. and Wyllie P. J. (1986) Phase relationships of gabbro–tonalite–granite–water at 15 kbar with applications to differentiation and anatexis. *Am. Mineral.* **71,** 301–316.
Jarosewich E., Nelen J. A., and Norberg J. A. (1980) Reference samples for electron microprobe analysis. *Geostand. Newsl.* **4,** 43–47.
Kempton P. D., Downes H., Sharkov E. V., Vetrin V. R., Ionov D. A., Carswell D. A., and Beard A. (1995) Petrology and geochemistry of xenoliths from the Northern Baltic Shield: Evidence for partial melting and metasomatism in the lower crust beneath an Archean terrane. *Lithos* **36,** 157–184.
Kinzler R., Grove T. L., and Recca S. I. (1990) An experimental study on the effect of temperature and melt composition on the partitioning of nickel between olivine and silicate melt. *Geochim. Cosmochim. Acta* **54,** 1255–1265.
Klein M., Stosch H.-G., and Sack H. A. (1997) Partitioning of high field-strength and rare-earth elements between amphibole and quartz-dioritic to tonalitic melts: an experimental study. *Chem. Geol.* **138,** 257–271.
LaTourrette T., Hervig R. L., and Holloway J. R. (1995) Trace element partitioning between amphibole, phlogopite, and basanite melt. *Earth Planet. Sci. Lett.* **135,** 13–30.
Leake B. E. (1997) Nomenclature of amphiboles: Report of the subcommittee on amphiboles of the international mineralogical association, commission on new minerals and mineral names. *Can. Mineral.* **35,** 219–246.
McKay G. A., Wagstaff J., and Yang S. R. (1986) Clinopyroxene REE distribution coefficients for shergottites: The REE content of the Shergotty melt. *Geochim. Cosmochim. Acta* **50,** 927–937.
Michael P. J. (1988) Partition coefficients for rare earth elements in mafic minerals of high silica rhyolites: The importance of accessory mineral inclusions. *Geochim. Cosmochim. Acta* **52,** 275–282.
Mysen B. O. and Boettcher A. L. (1975) Melting of a hydrous mantle: II. Geochemistry of crystals and liquids formed by anatexis of mantle peridotite at high pressures and high temperatures as a function of controlled activities of water, hydrogen, and carbon dioxide. *J. Petrol.* **16,** 549–593.
Mysen B. O. (1983) The structure of silicate melts. *Ann. Rev. Earth Planet. Sci.* **11,** 75–97.
Nicholls I. A. and Harris K. L. (1980) Experimental rare earth element partition coefficients for garnet, clinopyroxene and amphibole coexisting with andesitic and basaltic liquids. *Geochim. Cosmochim. Acta* **44,** 287–308.
Nielsen C. H. and Sigurdsson H. (1981) Quantitative methods for electron microprobe analysis of sodium in natural and synthetic glasses. *Am. Mineral.* **66,** 547–552.
Nielsen R. L. (1985) A method for the elimination of the compositional dependence of trace element distribution coefficients. *Geochim. Cosmochim. Acta* **49,** 1775–1779.
Nielsen R. L. (1988) A model for the simulation of combined major and trace element liquid lines of descent. *Geochim. Cosmochim. Acta* **52,** 27–38.
Nielsen R. L. (1990) Simulation of igneous differentiation processes, In *Modern Methods of Igneous Petrology* (eds. J. Nichols and J. K. Russell), *MSA Rev. Mineral.* **23,** 65–105.
Nielsen R. L. and Beard J. S. (in press) Magnetite-melt HFSE partitioning. *Chem. Geol.*
Nielsen R. L. and Dungan M. A. (1983) The Petrology and geochemistry of the Ocate Volcanic Field, north-central New Mexico. *Geol. Soc. Amer. Bull.* **96,** 296–312.
Nielsen R. L. Forsythe L. M., Gallaghan W. E., and Fisk M. R. (1994) Major and trace element magnetite-melt partitioning. *Chem. Geol.* **117,** 167–191.
Nielsen R. L., Gallaghan W. E., and Fisk M. R. (1992) The partitioning of Sc, Y, and the REE between olivine, low-Ca pyroxene, ilmenite, magnetite and natural silicate magmas. *Contrib. Mineral. Petrol.* **110,** 488–499.
Oberti, R., Bottazzi P., Tiepolo M., Vannucci R., Zanetti A., and Foley S. (1999a) Compositional and structural constraints on trace-element partitioning: An integrated approach. *EOS* **80,** S362 (abstr.).
Oberti R., Hawthorne F. C., Camara F., and Raudsepp M. (1999b) Unusual M3+ cations in synthetic amphiboles with nominal fluoroeckermannite composition: Deviations from stoichiometry and structural effects of the cummingtonite component. *Am. Mineral.* **84,** 102–111.
Onuma N., Higuchi H., and Wakita H. (1968) Trace element partition between two pyroxenes and the host volcanic rocks. *Earth Planet. Sci. Lett.* **5,** 47–51.
Patinõ-Douce A. E. and Beard J. S. (1995) Dehydration melting of biotite gneiss and quartz amphibolite from 3 to 15 kbar. *J. Petrol.* **36,** 707–738.
Patinõ-Douce M. L., Patinõ-Douce A., Qayyum, M., and Nielsen R. L. (1994) A new set of low concentration standards for La, Ce, Sm, Yb, Lu, Y, Sc, V, Nb, and Ta in silicates. *Geostand. Newslett.* **18,** 195–198.
Rapp R. P. (1995) Amphibole-out phase boundary in partially melted metabasalt, its control over liquid fraction and composition, and source permeability. *J. Geophys. Res.* **100,** 15,601–15,610.
Rapp R. P. and Watson E. B. (1995) Dehydration melting of metabasalt at 8–32 kbar: Implications for continental growth and crust-mantle recycling. *J. Petrol.* **36,** 891–931.
Robinson P., Schumacher J. C., and Spear F. S. (1982) Phase relations of metamorphic amphiboles: Natural occurrence and theory. In *Amphiboles: Petrology and experimental phase relations* (eds. Veblen, D. and Ribbe, R.), *MSA Rev. Mineral.* **9b**.
Romick D., Kay S. M., and Kay R. W. (1995) The influence of amphibole fractionation on the evolution of calc-alkaline andesite and dacite tephra from the central Aleutians, Alaska. *Contrib. Mineral. Petrol.* **112,** 101–118.
Rushmer T. (1991) Partial melting of two amphibolites: Contrasting experimental results under fluid absent conditions. *Contrib. Mineral. Petrol.* **107,** 41–59.
Rutherford M. J., Sigurdsson H., Carey S., and Davis A. (1985) The May 18, 1980 eruption of Mt. St. Helens, 1: Melt composition and experimental phase equilibria. *J. Geophys. Res.* **90,** 2929–2947.
Rutherford M. J. and Devine J. D. (1988) The May 18, 1980, eruption of Mt. St. Helens, 3. Stability and chemistry of amphibole in the magma chamber. *J. Geophys. Res.* **93,** 11,949–11,959.
Sajon F. G., Maury R. C., Bellon H., Cotten J., and Defant M. (1996) High Field Strength Element enrichment of Pliocene-Pleistocene island arc basalts, Zamboanga Peninsula, Western Mindanao (Philippines). *J. Petrol.* **37,** 693–726.
Shannon R. D. (1976) Revised effective ionic radii and systematic studies of interatomic distances on halides and chalcogenides. *Acta Crystal.* **32,** 751.
Sharma A. (1996) Experimentally derived thermochemical data for pargasite and reinvestigation of its stability with quartz in the system Na_2O–CaO–MgO–Al_2O_3–SiO_2–H_2O. *Contrib. Mineral. Petrol.* **125,** 263–275.
Sisson T. W. (1994) Hornblende-melt trace-element partitioning measured by ion microprobe. *Chem. Geol.* **117,** 331–344.
Sisson T. W. and Grove T. L. (1993) Experimental investigation of the role of H_2O in calc-alkaline differentiation and subduction zone magmatism. *Contrib. Mineral. Petrol.* **113,** 143–166.
Skjerlie K. P. and Johnston D. A. (1996) Vapor-absent melting from 10–20 kbar of crustal rocks that contain multiple hydrous phases: Implications for anatexis in the deep to very deep continental crust and active continental margins. *J. Petrol.* **37,** 661–691.
Spulber S. D. and Rutherford M. J. (1983) The Origin of rhyolite and plagiogranite in oceanic crust: An experimental study. *J. Petrol.* **24,** 1–25.
Tiepolo M., Vannucci R., Zanetti A., Brumm, R. C., Foley, S. F., Bottazzi P., and Oberti R. (1998) Fine scale structural control of REE site-preference: The case of amphibole. *Mineral. Mag.* **62A,** 1517–1518 (abstr.).
Watson E. B. (1985) Henry's Law behavior in simple systems and magmas: Criteria for determining concentration-dependent partition coefficients in nature. *Geochim. Cosmochim. Acta* **49,** 917–923.
Winther K. T. (1996) An experimentally based model for the origin of tonalitic and trondhjemitic melts. *Chem. Geol.* **27,** 43–59.

Wolf M. B. and Wyllie P. J. (1994) Dehydration-melting of amphibolite at 10 kbar: The effects of temperature and time. *Contrib. Mineral. Petrol.* **115,** 369–383.

Wones D. A. and Gilbert C. M. (1982) Amphiboles in the Igneous Environment. In: *Amphiboles: Petrology and Experimental Phase Relations.* (eds. Veblen and Ribbe), *MSA Rev. Mineral.* **9b,** pp. 355–390

Wood B. J. and Blundy J. D. (1997) A predictive model for rare earth element partitioning between clinopyroxene and anhydrous silicate melt. *Contrib. Mineral. Petrol.* **129,** 166–188.

Yang H., Konzett J., Prewitt, C. T., and Fei Y. (1999) Single crystal structure refinement of synthetic M_4K-substituted potassic richterite, $K(KCa)Mg_5Si_8O_{22}(H)_2$. *Am. Miner.* **84,** in press.

View publication stats